

THE 2004 AND 1861 TSUNAMI DEPOSITS ON SIMEULUE  
ISLAND, WESTERN SUMATRA

---

A Thesis

Presented to

The Graduate Faculty

Central Washington University

---

In Partial Fulfillment

of the Requirements for the Degree

Master of Science

Geology

---

by

Katherine Frances Whitlow

January 2008

CENTRAL WASHINGTON UNIVERSITY

Graduate Studies

We hereby approve the thesis of

Katherine Frances Whitlow

Candidate for the degree of Master of Science

APPROVED FOR THE GRADUATE FACULTY

---

Dr. Charles M. Rubin, Committee Chair

---

Dr. Lisa Ely

---

Dr. Beth Pratt-Sitaula

---

Associate Vice President of Graduate Studies

## ABSTRACT

### THE 2004 AND 1861 TSUNAMI DEPOSITS ON SIMEULUE ISLAND, WESTERN SUMATRA

by

Katherine Frances Whitlow

January 2008

Megathrust earthquakes and associated tsunamis along the subduction zone along western Sumatra represent a significant seismic hazard that is not well understood. I present the results of mapping, paleoseimologic, and geochronologic studies of tsunami deposits exposed on Simeulue Island, western Sumatra, to document the timing of past tsunamis. Three field sites were targeted to conduct these studies: Inor, Busong Bay, and Langi Bay. Stratigraphic relationships, geochronologic data, and grain size analyses from these field sites show evidence of a tsunami that occurred in 1861 following a  $M_w \sim 8.5$  earthquake. A wood fragment collected from an excavation at Inor yielded an age of 1640–1960 A.D. A coral boulder from an excavation at Busong Bay yielded an age of  $1868 \pm 19$  years. The 2004 tsunami deposit was also exposed in excavations at the three field sites. Identifying tsunami deposits and characterizing their stratigraphic and depositional settings will help to further understand tsunami inundation and preservation in the geologic record.

## ACKNOWLEDGMENTS

I thank Shige Fujino and Eko Yulianto for helping dig numerous holes, describing countless stratigraphic layers, and discussing various geological scenarios in the field. We made a great team! My advisor, Charlie Rubin, has been extremely helpful with editing and discussing my research. Thanks a million! I thank my committee: Charlie Rubin, Lisa Ely, and Beth Pratt-Sitaula. I thank Shige for completing grain size analyses on the Inor trenches and for submitting samples for AMS dating. I thank Aron Meltzner for his help surveying and his perpetual patience with explaining tidal data and coral dating to me. I thank Kerry Sieh for taking the role of advisor while we were in Sumatra and for making this research trip possible for me. I thank Rich Briggs, Dan Maxwell, and John Galetzka for helping me in the field and for the comic relief. This trip would not have been possible without the help of Bambang Suwargadi, who helped organize the logistics of this research trip on the Indonesian side. I thank my many Indonesian colleagues, including Imam Suprihanto, Nugraha Sastra, and Dudi Prayudi for field assistance. I thank all the above for the emotional support during the boat sinking and Putra's death. I know I wouldn't have made it without your help. Brian Atwater thankfully gathered some greatly needed field notes for me and allowed me to join him in the field along the Washington coast to see tsunami deposits prior to my Sumatra trip. I thank Hong-Wei Chiang, Chuan-Cou (River) Shen, and Larry Edwards for the U/Th dates. My wonderful family and friends provided their never-ending support, laughs, and advice through these past 2 years! I have the best friends and family on the planet! I have to thank Pearly, the best (and fattest) cat ever. She's a wonderful friend.

This work was funded in part by Caltech's Plate Boundary Observatory, Central Washington University, Active Fault Research Center, Geological Survey of Japan/AIST, and a grant-in-aid from the Geological Society of America.

## TABLE OF CONTENTS

| Chapter  | Page |
|--|------|
| I        INTRODUCTION.....   | 1    |
| Tectonic Setting.....  | 3    |
| Historic Record of Earthquakes and Tsunamis on Simeulue Island ..... | 5    |
| Tsunami Deposits .....   | 7    |
| II      METHODS, RESULTS, AND INTERPRETATION.....                    | 9    |
| Stratigraphy.....  | 10   |
| Geochronology .....  | 40   |
| Topographic Profiling.....   | 48   |
| III     DISCUSSION .....   | 53   |
| The 2004 Tsunami Deposits .....                                      | 53   |
| The Candidate 1861 Tsunami Deposits.....                             | 55   |
| Tsunami Sands and Coseismic Uplift.....                              | 58   |
| IV     CONCLUSIONS.....  | 61   |
| REFERENCES .....   | 62   |

## LIST OF TABLES

| Table  | Page |
|--|------|
| 1      Historical Megathrust Earthquakes Along the Sumatran Subduction Zone<br>Near Simeulue Island..... | 6    |
| 2      Busong Bay Tsunami-Derived Coral Boulders .....   | 34   |
| 3      Radiocarbon Analyses .....  | 43   |
| 4      Uranium and Thorium Isotopic Compositions and $^{230}\text{Th}$ Analyses.....                     | 47   |
| 5      Heights of the Candidate 1861 and 2004 Tsunami Sands Above the<br>2006 Annual Low Tide.....       | 52   |

## LIST OF FIGURES

| Figure |   | Page |
|--------|---|------|
| 1      | Location map of study area.....   | 2    |
| 2      | Map of field locations and coseismic land level changes on Simeulue Island .....  | 4    |
| 3      | Schematic of a subduction zone rupturing and forming a tsunami.....   | 5    |
| 4      | Geomorphology of Inor.....  | 11   |
| 5      | Inor fence diagram of trenches A, B, F, D, E, and I .....   | 13   |
| 6      | Inor trench A stratigraphy and AMS radiocarbon ages.....  | 15   |
| 7      | Inor trench B stratigraphy.....   | 16   |
| 8      | Inor trench D stratigraphy.....   | 17   |
| 9      | Inor trench E stratigraphy .....  | 18   |
| 10     | Inor trench I stratigraphy .....  | 20   |
| 11     | Inor trench F stratigraphy .....  | 21   |
| 12     | Sample location for grain size analysis of the 1861 tsunami deposit, trench F, Inor.....  | 22   |
| 13     | A schematic diagram of a settling tube .....  | 22   |
| 14     | Graphical analyses (weight percent versus phi) and statistics of the candidate 1861 tsunami sands in Inor trenches A and B .....  | 24   |
| 15     | Graphical analyses (weight percent versus phi) and statistics of the candidate 1861 tsunami sand in Inor trenches F, E, D, and I .....  | 25   |
| 16     | Graphical analyses (weight percent versus phi) and statistics of modern beach sand at Inor, substrate material (unit directly below the candidate 1861 tsunami sand) from trenches E and L, parallel laminated sand from trench L, and cross-stratified sand from trench J..... | 26   |

## LIST OF FIGURES (continued)

|    |   |    |
|----|---|----|
| 17 | Grain size analysis of Inor trench D.....   | 27 |
| 18 | Geomorphology of Busong Bay .....   | 31 |
| 19 | Busong Bay trench A stratigraphy .....  | 32 |
| 20 | Busong Bay coral boulder tsunami deposits.....  | 34 |
| 21 | Geomorphology of Langi Bay .....  | 36 |
| 22 | Langi Bay trench E stratigraphy .....   | 38 |
| 23 | Langi Bay trench A stratigraphy.....  | 39 |
| 24 | Langi Bay trench D stratigraphy.....  | 41 |
| 25 | Langi Bay fence diagram of trenches D, A, and E .....   | 42 |
| 26 | Busong Bay trench A U–Th sample.....  | 46 |
| 27 | Langi Bay and Inor topographic profiles.....  | 50 |
| 28 | Busong Bay topographic profiles.....  | 51 |
| 29 | Busong Bay Trench B showing sub-layers and minor flame<br>structures within the 2004 tsunami sand, looking north..... | 54 |
| 30 | Rip-up clasts at the base of unit 2, trench E, Inor .....   | 57 |
| 31 | Rip-up clasts within unit 2, trench F, Inor.....  | 57 |
| 32 | Coseismic land level changes and tsunami sand thickness isopachs on<br>Simeulue Island.....                           | 60 |

## CHAPTER I

### INTRODUCTION

The December 26, 2004  $M_w$  9.2 Sumatra-Andaman earthquake was one of the largest earthquakes recorded in the past century and resulted in a catastrophic tsunami that caused over 300,000 fatalities (McCloskey *et al.*, 2005). Shortly following this event, on March 28, 2005, an  $M_w$  8.7 earthquake occurred, generating another tsunami (Figure 1). These earthquakes and ensuing tsunamis triggered various questions, including the recurrence interval of great ( $M_w > 8$ ) earthquakes along the Sumatran subduction zone and the magnitude and frequency of tsunami inundation.

Identifying deposits from recent and past tsunamis along the Sunda megathrust will provide a more accurate tsunami record for northwestern Sumatra and nearby islands. By characterizing the sedimentology and stratigraphy of tsunami deposits on Simeulue Island, tsunami run-up heights and inundation models will be better constrained. Uplift and subsidence from great megathrust earthquakes in western Sumatra have been previously documented in the region by coral microatoll studies (Zachariasen *et al.*, 1999; Zachariasen *et al.*, 2000; Natawidjaja *et al.*, 2004; Briggs *et al.*, 2006; Meltzner *et al.*, 2006; Subarya *et al.*, 2006), but the timing of past tsunamis on Simeulue Island, western Sumatra, is poorly documented (Figure 1).

Simeulue Island, located about 100km northeast of the subduction zone interface, is an ideal location for studying tsunami deposits and deformation associated with great earthquakes. Following the 2004  $M_w$  9.2 earthquake, the northern region of Simeulue Island experienced up to 150cm of uplift, while the southern region experienced up to

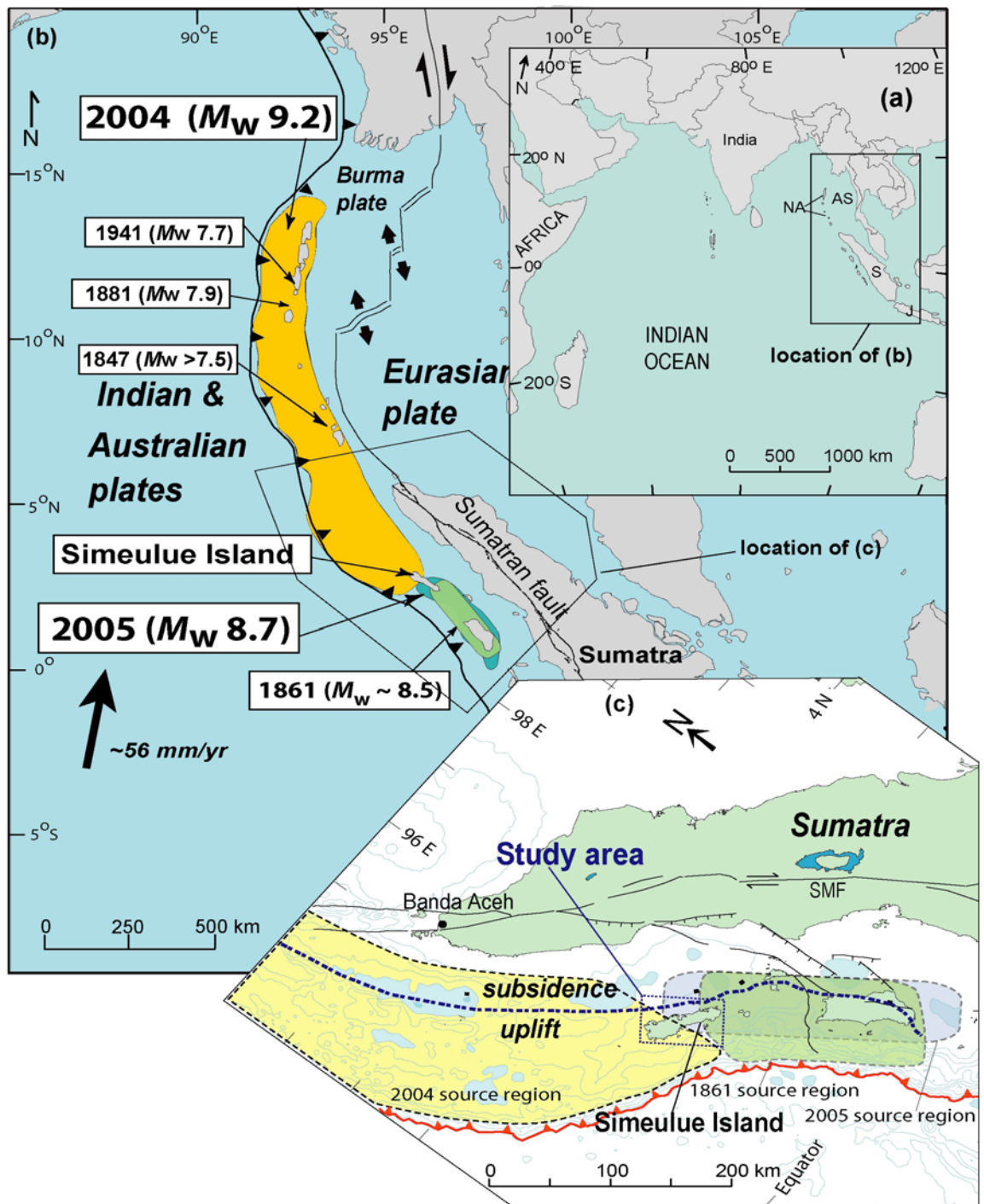


Figure 1. Location map of study area. (a) Indian Ocean basin. S, Sumatra; J, Java; NA, Nicobar-Andaman Islands; AS, Andaman Sea. (b) Map of past earthquakes along the Sunda megathrust. (c) Pivot line between uplift and subsidence during the 2004 earthquake. The 2004 source region, yellow; the 2005 source region, blue; the 1861 source region, green. SMF, Sumatran fault zone. Modified from Briggs *et al.*, 2006, Subarya *et al.*, 2006, Bilham *et al.*, 2005, Bock *et al.*, 2003, and Walker *et al.*, 2005.

30cm of subsidence; the 2005 event resulted in the northern region remaining stable with over 150cm of emergence in the southern part of the island (Figure 2; Briggs *et al.*, 2006; Meltzner *et al.*, 2006).

My objectives were to document recent and past tsunami-derived sand deposits on Simeulue Island (Figure 1). I characterized the geomorphic setting of three sites: Inor, Busong Bay, and Langi Bay on Simeulue Island (Figure 2) through detailed field mapping, stratigraphic descriptions of trench wall exposures, sedimentologic analyses, and geochronology. Constraining the timing of the penultimate tsunami will help document the repeat time for future tsunamis generated by large ruptures along the Sunda megathrust.

### Tectonic Setting

The island of Sumatra is located along the Eurasian and subducting Indo-Australian plate boundary (Figure 1). The arcuate subduction zone (i.e. the Sunda megathrust) is over 5600km and extends from the north Andaman Sea along the west coast of Sumatra, bending east south of Java (Figure 1). Along the western coast of Sumatra, the Indo-Australian plate is subducting obliquely beneath the Sunda plate (the continental shelf of Southeast Asia). Plate parallel motion is accommodated by dextral slip along the Sumatran fault zone about 200km east of the Sunda megathrust (Figure 1). The dip of the subducting Indo-Australian plate is about  $12^\circ$  at the plate interface (Dewey *et al.*, 2007), increases to  $17.5^\circ$  below northwest Simeulue Island (Dewey *et al.*, 2007), and then to about  $50^\circ$  below the Sumatran fault zone (Newcomb and McCann, 1987).

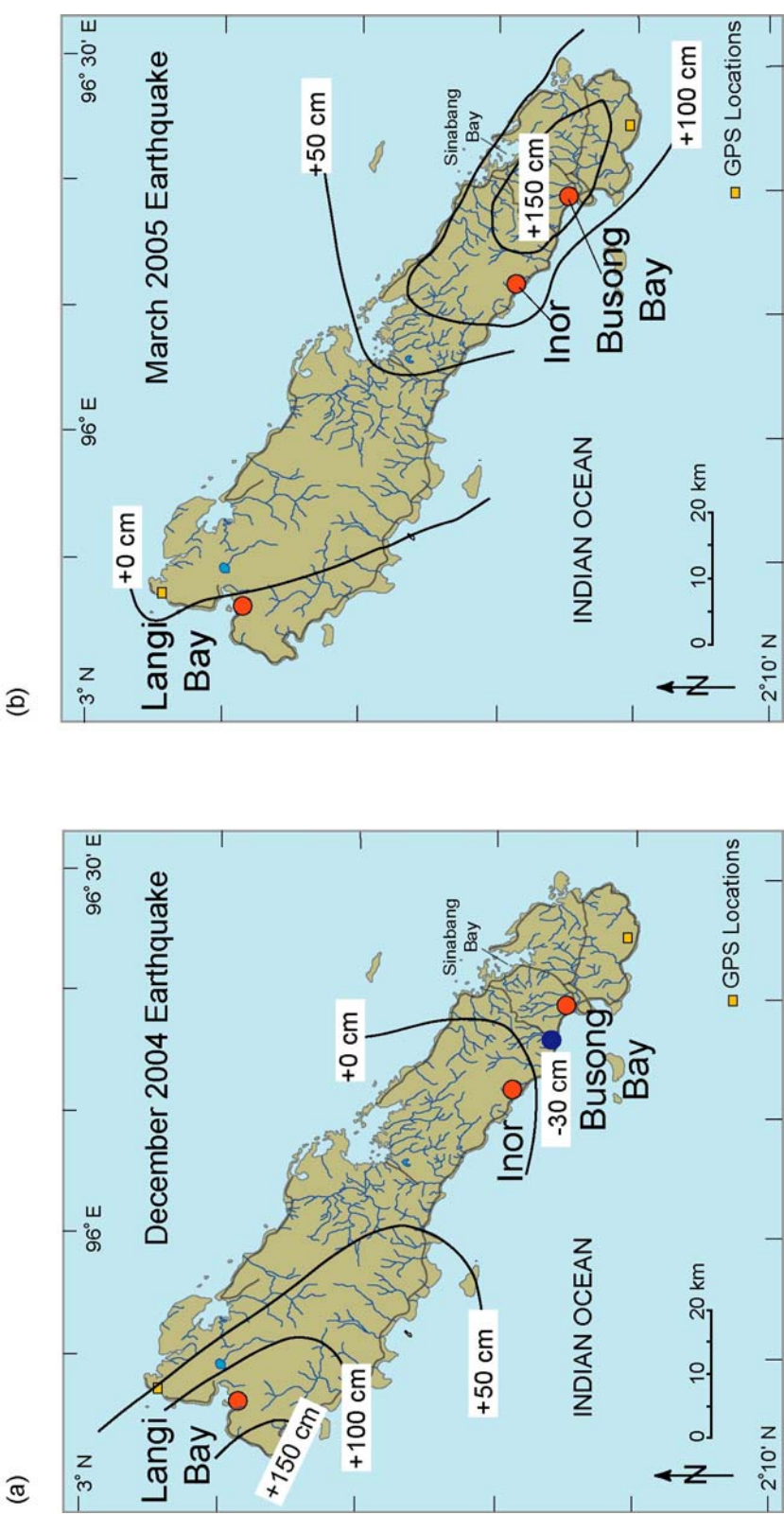


Figure 2. Map of field locations and coseismic land level changes on Simeulue Island. (a) Uplift associated with the December 26, 2004 earthquake as determined from Global Positioning System (GPS). (b) Uplift associated with the March 28, 2005 earthquake on the island as determined from GPS. Modified from Briggs *et al.*, 2006.

At the latitude of Simeulue Island, the plates are converging at about 53 mm/yr (Bock *et al.*, 2003).

### Historic Record of Earthquakes and Tsunamis on Simeulue Island

Tsunamis are typically generated by surface displacement on the sea floor from rupture along the megathrust interface in subduction zone settings (Atwater *et al.*, 2005). Here, the seafloor is displaced, resulting in the movement of the overlying ocean waters, forming a tsunami (Figure 3).

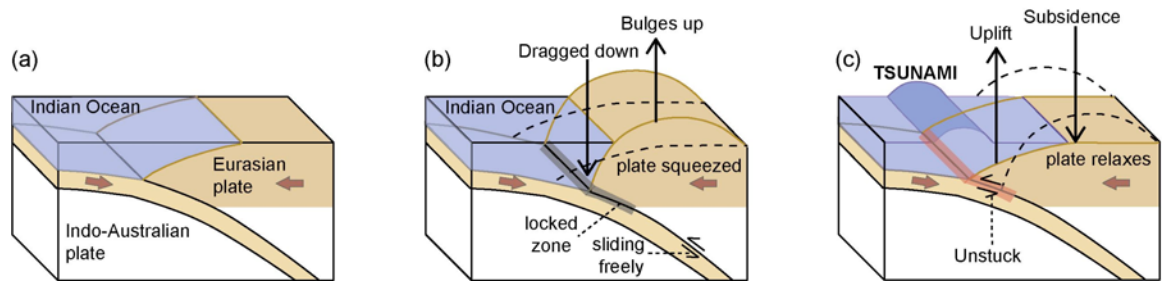


Figure 3. Schematic of a subduction zone rupturing and forming a tsunami. (a) Initial condition. (b) Interseismic emergence offshore and subsidence onshore. (c) Coseismic generation of tsunami, with local uplift onshore and oceanward subsidence. Modified from Atwater *et al.*, 2005.

Both recent and past tsunamis have inundated the coast of Simeulue Island, western Sumatra (Figure 1 and Table 1). According to our recent reconnaissance studies and interviewing of local residents, Simeulue Island experienced tsunami inundation in 2005, 2004, 1907, and 1861 (E. Yulianto, personal comm., 2006; Newcomb and McCann, 1987). In 2005, tsunami heights at Inor were about 1.5m high (E. Yulianto, personal comm., 2006). At Langi Bay, tsunami victims were found in coconut trees, implying tsunami heights of over 6m (E. Yulianto, personal comm., 2006). In 2004, local

Table 1  
Historical Megathrust Earthquakes Along the Sumatran Subduction Zone Near Simeulue Island

| Date           | Latitude<br>(°) | Longitude<br>(°) | $M_w$   | Rupture<br>Length (km) | Maximum<br>Vertical Slip<br>(m) | Reference  |
|----------------|-----------------|------------------|---------|------------------------|---------------------------------|--|
| March 28, 2005 | 2.0             | 96.8             | 8.7     | ~400                   | ~11                             | Briggs <i>et al.</i> (2006);<br>Walker <i>et al.</i> (2005)              |
| Dec. 26, 2004  | 3.2             | 95.8             | 9.2     | ~1600                  | ~20                             | Subarya <i>et al.</i> (2006);<br>Meltzner <i>et al.</i> (2006)           |
| Nov. 2, 2002   | 2.8             | 96.1             | 7.3     | ~70                    |                                 | DeShon <i>et al.</i> (2005);<br>Briggs <i>et al.</i> (2006)              |
| June 26, 1941  | 12.1            | 92.5             | 7.7     |                        |                                 | R. Bilham, personal comm. (2007);<br>Krishnan (1953); Jhingram (1953)    |
| Dec. 1935      | -0.3            | 98.3             | 7.7     | ~65                    | ~3                              | Natawidjaja <i>et al.</i> (2004); Rivera <i>et<br/>al.</i> (2002)        |
| Jan. 4, 1907   | 2.0             | 96.8             | 7.6     |                        |                                 | Newcomb and McCann (1987)  |
| Dec. 31, 1881  | 9.3             | 92.5             | 7.9     |                        |                                 | R. Bilham, personal comm.<br>(2007); Krishnan (1953);<br>Jhingram (1953) |
| Feb. 16, 1861  | 2.0             | 96.8             | 8.3–8.5 | ~400                   |                                 | Newcomb and McCann (1987);<br>Walker <i>et al.</i> (2005)                |
| Oct. 31, 1847  | 7.0             | —                |         | >7.5                   |                                 | R. Bilham, personal comm.<br>(2007); Krishnan (1953); Jhingram<br>(1953) |

residents experienced tsunami heights of 2m in Busong Bay. In 1861, rupture along a 250-km-long segment of the Sunda megathrust between 0° and 2.5° N produced an  $\sim M_w$  8.5 earthquake and generated tsunami waves that traveled over 500km from the source region with wave heights up to 7m in some areas (Newcomb and McCann, 1987). North of the 2004 rupture, several historic earthquakes ( $M_w > 7.9$ ) occurred along the Nicobar-Andaman plate boundary in 1847, 1881, and 1941 (R. Bilham, personal comm., 2007; Krishnan, 1953; Jhingram, 1953). Aftershocks following the 2004 earthquake suggest that the rupture zones of 1847, 1881, and 1941 Nicobar-Andaman earthquakes re-ruptured during the 2004 earthquake.

### Tsunami Deposits

Tsunami deposits are typically preserved in quiet coastal settings, such as estuarine or lagoon environments (Atwater and Moore, 1992; Kelsey *et al.*, 2005; Dawson, 1994; Minoura *et al.*, 1996; Cisternas *et al.*, 2005; Nanayama *et al.*, 2003). In these settings, tsunamigenic sands are interbedded with organic-rich mud and peat from the estuary or lagoon (Kelsey *et al.*, 2005; Minoura *et al.*, 1996). In quiet depositional environments where erosion is minimal, deposition of silt and clay-sized sediments are common, whereas sand and coarser materials are deposited only during storm surges, terrestrial floods, or tsunamis. Unfortunately, storm and terrestrial flood deposits look similar to tsunami deposits. However, in equatorial regions, large tropical storm surges are not a candidate for sand deposition. In order for tropical storms to form, ocean temperatures must be between 25° and 30° C, the atmosphere must undergo rotation facilitated by trade winds, and a Coriolis force needs to exist to create a vortex (Bryant, 1997). Since the

Coriolis force does not occur within 5° north or south of the equator (Bryant, 1997), Simeulue Island and northwest Sumatra will not experience storm surges generating large tropical storms, eliminating the possibility of storm-derived deposits.

## CHAPTER II

### METHODS, RESULTS, AND INTERPRETATION

Prior to the 2006 field season, field sites were targeted based on the geomorphology and depositional environments along the west coast of Simeulue Island, western Sumatra (Figure 2). Three locations on Simeulue Island were selected: Inor, Busong Bay, and Langi Bay (Figure 2). Inor was targeted in order to characterize tsunami inundation in a river-dominated environment. Busong Bay and Langi Bay were targeted in order to understand tsunami inundation in coastal bay environments. All three sites experienced tsunami inundation in the aftermath of the 2004 and 2005 earthquakes. Local residents and previous research by Newcomb and McCann (1987) show evidence of an  $M_w \sim 8.5$  earthquake and tsunami in 1861 that inundated Simeulue Island. An older candidate tsunami sand was found in excavations on Simeulue Island and will be referred to as the candidate 1861 tsunami sand.

In order to determine whether the sand is derived from a tsunami or a terrestrial flood, three lines of evidence are required: (1) bracketing the age of the sand layer with geochronology methods determines if the sand layer coincides with a known large subduction zone earthquake, (2) paleoecologic analyses on fauna (e.g., diatoms and foraminifera) enveloped within the sand determines whether the sand is terrestrial or marine in origin, and (3) quantitative grain size analyses matching the candidate tsunami sand to the nearby beach sand verifies that the sands are marine derived. Along with eyewitness accounts, these methods confirm that candidate tsunami sand deposits

exposed on Simeulue Island are marine in origin (Morton *et al.*, 2007; Dawson, 1994; Moore *et al.*, 2006; Minoura *et al.*, 1996).

Beach parallel trenches (1–2 m) were excavated to document lateral variations within coastal stratigraphic deposits. Sand-size samples were collected for grain size analyses. In order to determine the timing of tsunami sand inundation, detrital charcoal and woody debris were analyzed using the AMS radiocarbon method. U–Th methods were used on detrital coral fragments within candidate tsunami deposits. Depths of stratigraphic layers within excavations and topographic profiling were completed using a Total Station. Geomorphic and modern features such as rivers, terraces, and roads were mapped using a handheld GPS.

#### *Stratigraphy*

##### Inor

Inor was targeted in order to characterize tsunami inundation in a river-dominated environment. Thirteen excavations were made in an abandoned rice paddy east of the Inor River and about 200m inland from the Indian Ocean (Figure 4). The stratigraphy of each trench was described in detail and samples were collected for grain size analyses and AMS radiocarbon dating. The stratigraphic units throughout trench excavations at Inor correlate relatively well (Figure 5).

There are three major stratigraphic units at Inor (Figure 6). Unit 1, the stratigraphic base, is a bioturbated blue to gray clay containing roots. Unit 2 overlays unit 1, and is a medium to coarse sand containing shell fragments, rip-up clasts, and minor laminations, and has a sharp lower boundary that dips slightly seaward. Unit 2

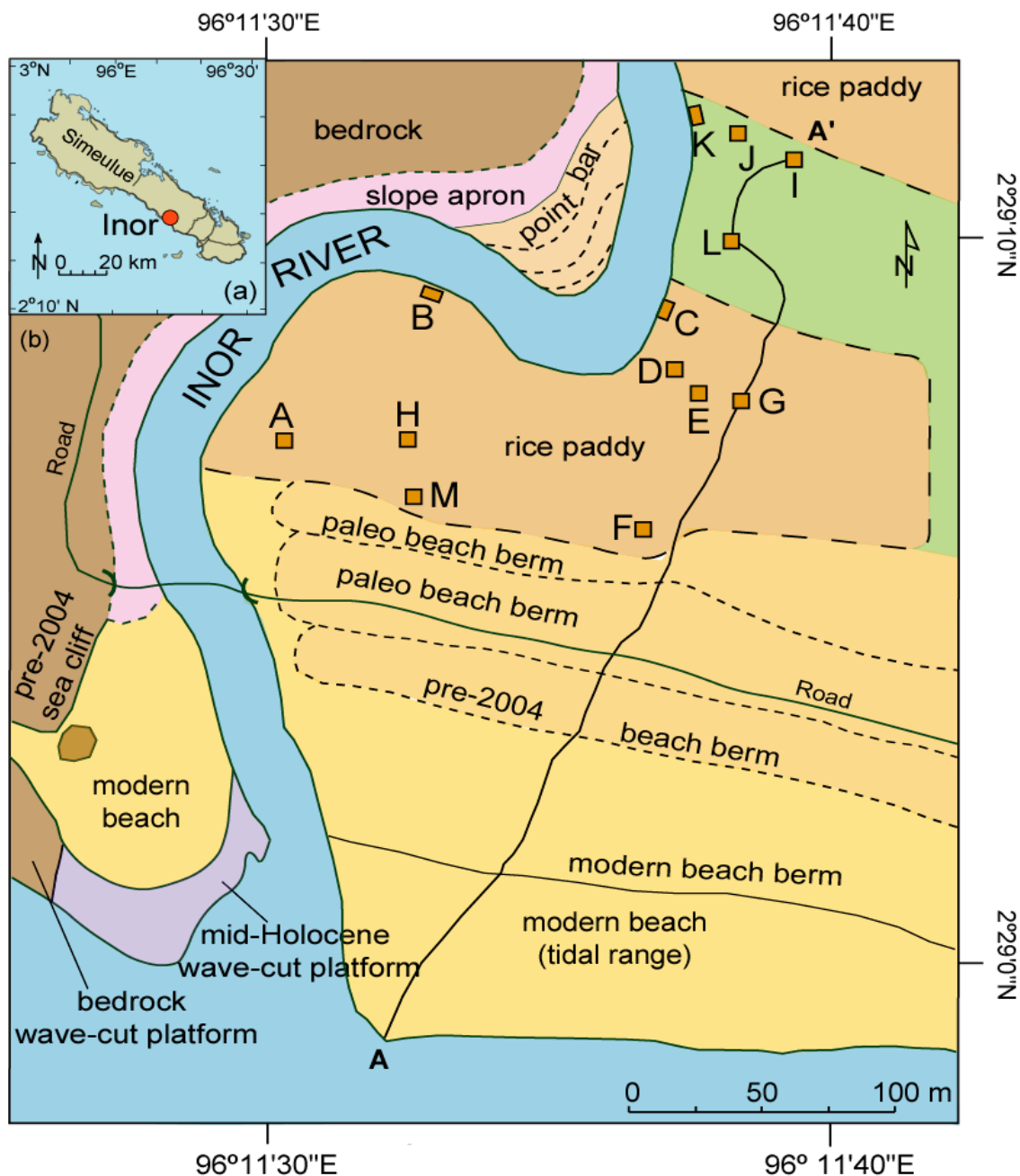


Figure 4. Geomorphology of Inor. (a) Location of Inor on Simeulue Island. (b) Inor geomorphology.

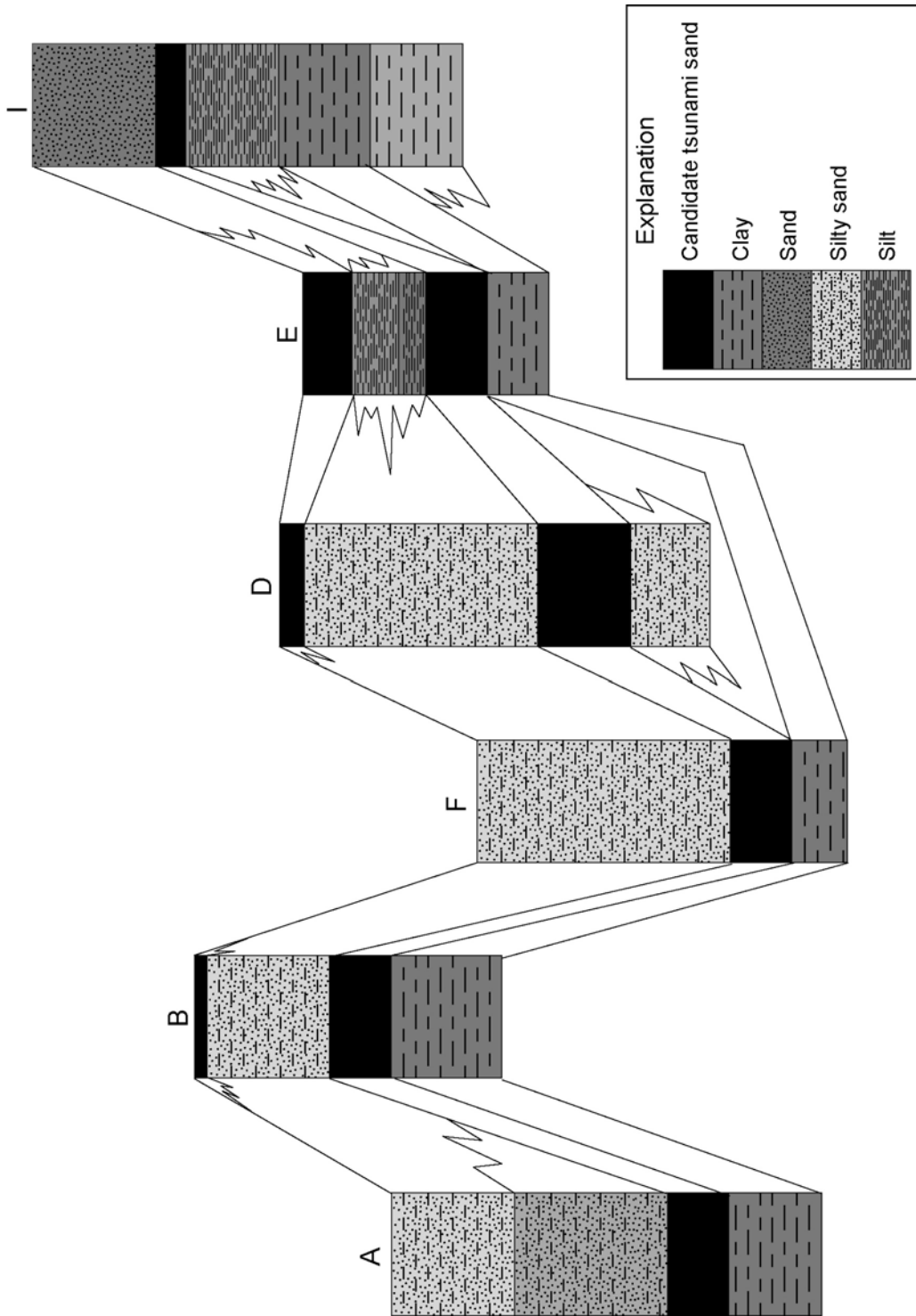


Figure 5. Inor fence diagram of trenches A, B, F, D, E, and I (see Figure 4 for trench locations).

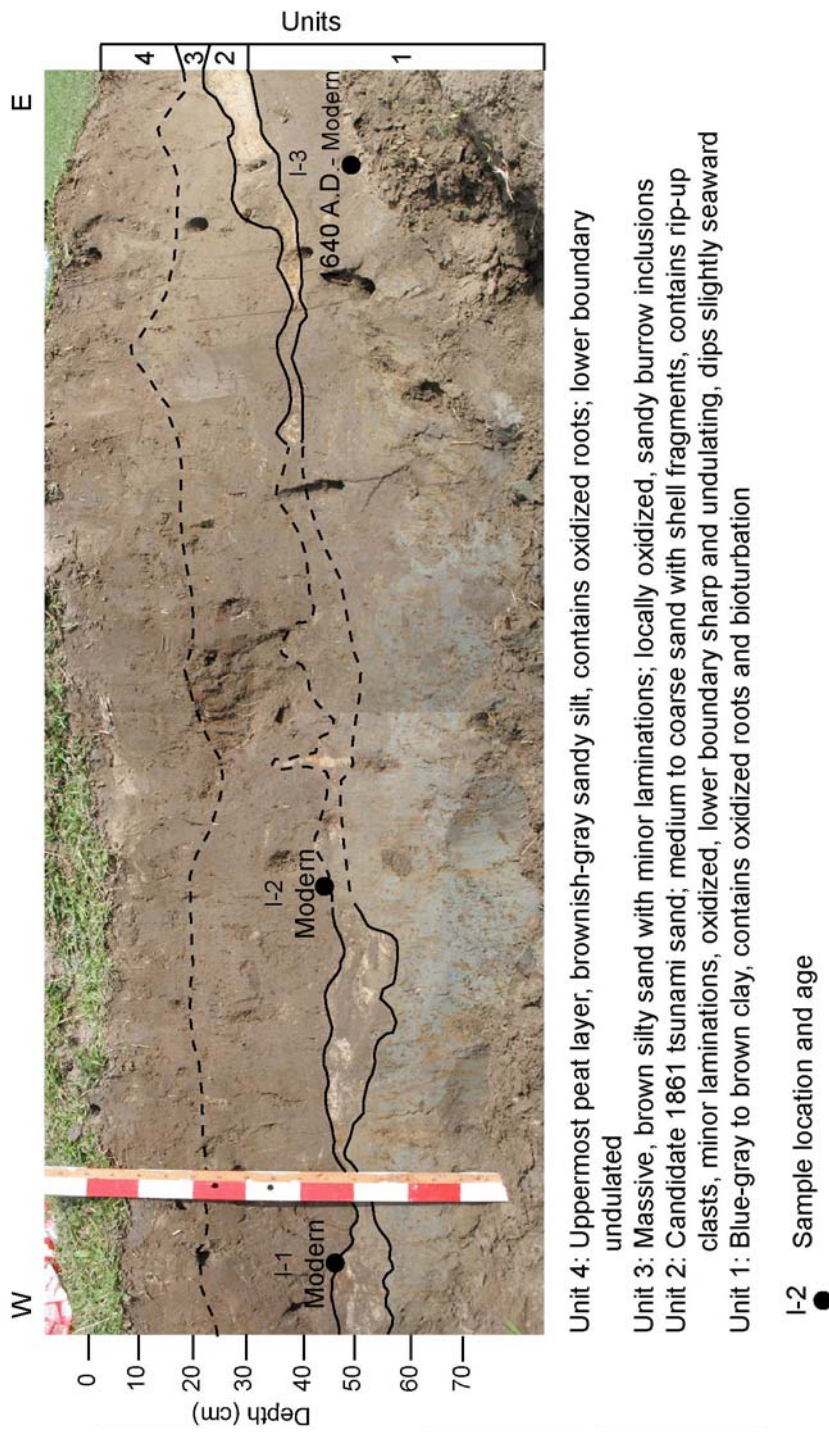


Figure 6. Inor trench A stratigraphy and AMS radiocarbon ages (see Figure 4 for trench location).

represents a candidate 1861 tsunami sand and is exposed in trenches A, B, D, E, F, and I. The candidate 1861 tsunami sand is exposed in trenches A, B, D, E, F, and I. Unit 3 and unit 4 represent the stratigraphic top of the various trenches at Inor and are likely composed of river-derived sediments. The 2004 tsunami sand is discontinuous at Inor. In trenches B and D, the 2004 tsunami sand overlies unit 3 (Figures 7 and 8) and overlies unit 4 in trench E (Figure 9).

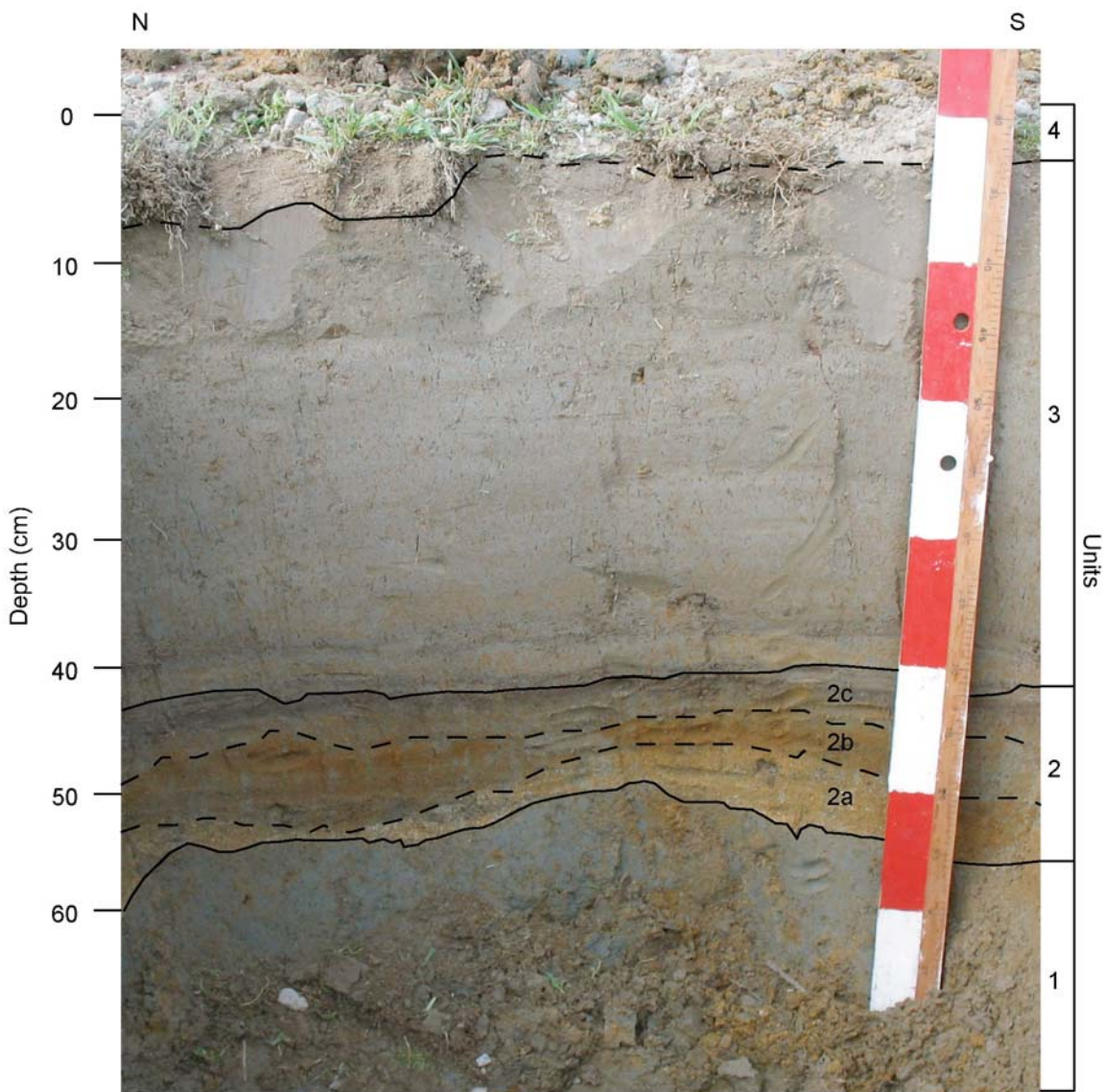
All of the trenches excavated at Inor are in an abandoned rice paddy where river flooding probably occurs regularly. The fine grain size of unit 1 (e.g., clay) indicates deposition in a low-velocity environment (Reading, 1996). The blue to gray color suggests water-rich conditions and reducing pore water (Reading, 1996). The existence of oxidized roots in the blue-gray clay and silt exposed in trench A unit 1 implies that it is a paleosol (Figure 6) and was most likely the paleo surface prior to the 1861 earthquake. Water buffalo and fresh-water insects probably caused the bioturbation within the clay unit. In trench B, the clay layer is oxidized from previous exposure to atmospheric oxygen (Figure 7). In trench I, the weak lamination in the unit 1 clay probably formed from silt falling out from suspension in a quiet water setting, similar to lake or coastal lagoon deposition (Figure 10).

Unit 2, the candidate 1861 tsunami sand, overlies unit 1 and consists of 15cm-thick, medium to coarse, stratified, poorly to well-sorted sand. This unit was deposited up to 360m inland (Figure 4). Shell fragments and gastropods found within the sand imply a marine origin. Unit 2 is thickest in trenches B and D, which are closest to the Inor River (Figure 4). When tsunamis return to the ocean, they tend to follow



Unit 4: 2004 tsunami deposit; White fine-grained well sorted sand  
Unit 3: Massive brown sandy silt, minor fine to medium sand lenses; undulating lower boundary  
Unit 2: Candidate 1861 tsunami sand; Subunit 2b: 5-7 cm, white to gray fine to medium grained sand, fines upwards to fine to medium sandy silt, upper boundary undulating, contains weak laminations. Subunit 2a: 3-6 cm, white to gray fine to medium grained sand, fines upwards to fine to medium sandy silt, lower boundary undulating, root laying on top of unit  
Unit 1: Brownish-red oxidized clay layer, bioturbated with burrows and roots, massive

Figure 7. Inor trench B stratigraphy (see Figure 4 for trench location).



Unit 4: 2004 tsunami deposit; Well sorted white to tan fine to medium sand

Unit 3: Massive gray sandy silt, massive, contains oxidized roots

Unit 2: Candidate 1861 tsunami sand; Subunit 2c: 2-3 cm, Laminated gray to dark gray clay. Subunit 2b: 1-2 cm, Oxidized orange and gray sandy silt. Subunit 2a: 2-6 cm, Orange to tan medium to coarse sand, with shell fragments

Unit 1: Blue-gray sandy silt, contains oxidized roots

Figure 8. Inor trench D stratigraphy (see Figure 4 for trench location).



Unit 5: 2004 tsunami sand; Massive white to tan fine to medium sand

Unit 4: Massive tan to brown silt, contains roots

Unit 3: Bluish-gray silt, contains burrows

Unit 2: Candidate 1861 tsunami sand: tan sand, fines upwards from medium sand to sandy silt, contains gastropods, lower boundary undulating, rip-up clasts within, flame structures at lower boundary

Unit 1: Blueish-gray clay, massive, contains some woody fragments, oxidized in places

Figure 9. Inor trench E stratigraphy (see Figure 4 for trench location).

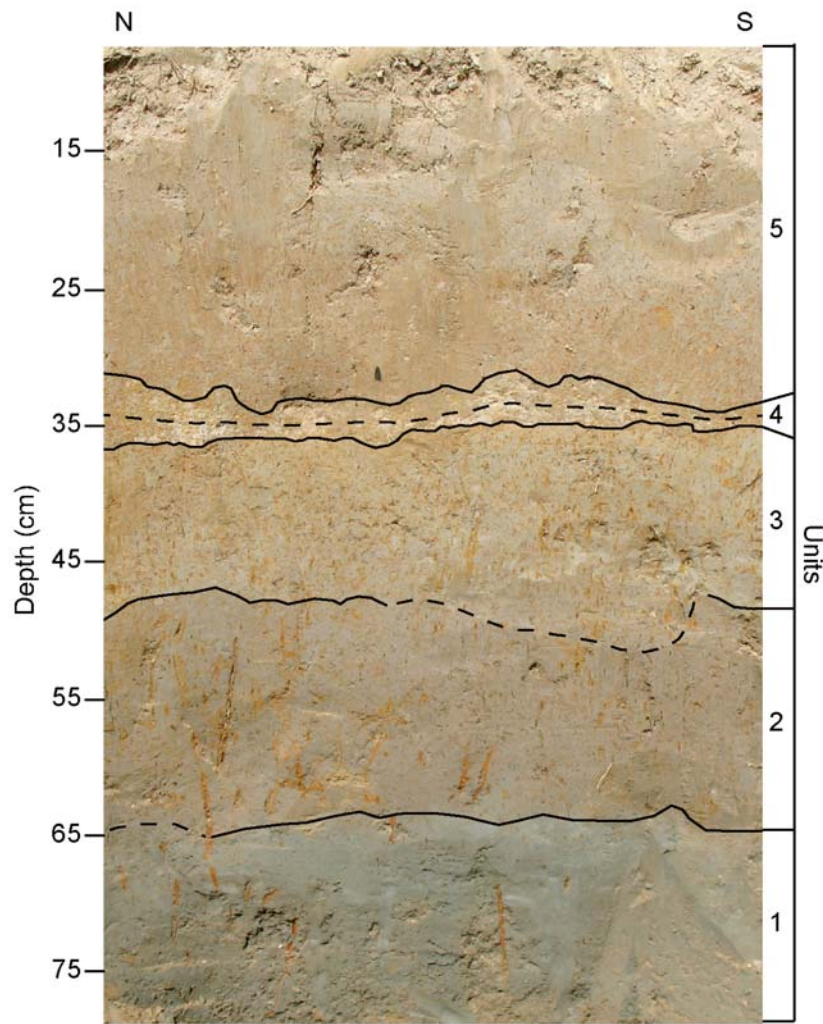


Figure 10. Inor trench I stratigraphy (see Figure 4 for trench location).

topographic lows, or the path of least resistance (Morton *et al.*, 2007). Since the Inor River is a topographic low, this provides a return path following the tsunami surge. The candidate 1861 tsunami sand is only 0 to 5cm thick in trench I, which is the farthest excavation from the Indian Ocean (Figure 4). This is consistent with other studies that document thinning of tsunami sand sheets inland from the modern shoreline (Minoura *et al.*, 1996; Benson *et al.*, 1997; Moore *et al.*, 2006; Morton *et al.*, 2007). The greatest thickness variability of the candidate 1861 tsunami sand is recorded in trenches E and F, at 0 to 11cm thick (Figure 9) and 3 to 11cm thick (Figure 11), respectively. The discontinuity of sand thickness between trenches probably resulted from either barriers that prevented deposition (such as trees, old beach berms, or houses), or erosion from wind and rain following deposition.

Stratigraphically above the candidate 1861 tsunami sand in trenches B, D, and E lies unit 3, a massive brown to gray sandy silt. Based on the grain size of this unit, it was likely deposited in a low-velocity environment (Boggs, 2001). The brown color possibly represents interaction with the atmosphere following deposition, when this unit was the ground surface. The gray color represents a standing water environment (Reading, 1996). Unit 3 likely was deposited as a result of the flooding of the Inor River, accounting for the gray color. The gray and brown colors indicate that the rice paddies at Inor probably experienced periods of both flooding and periodic drought.

The 2004 tsunami sand is discontinuous at Inor. Interestingly, the 2004 tsunami sand is only about 1 cm thick in trenches B and D (Figures 7 and 8) and is 3 to 5 cm thick in trench E (Figure 9). These variations in thickness may be due to a topographic low of

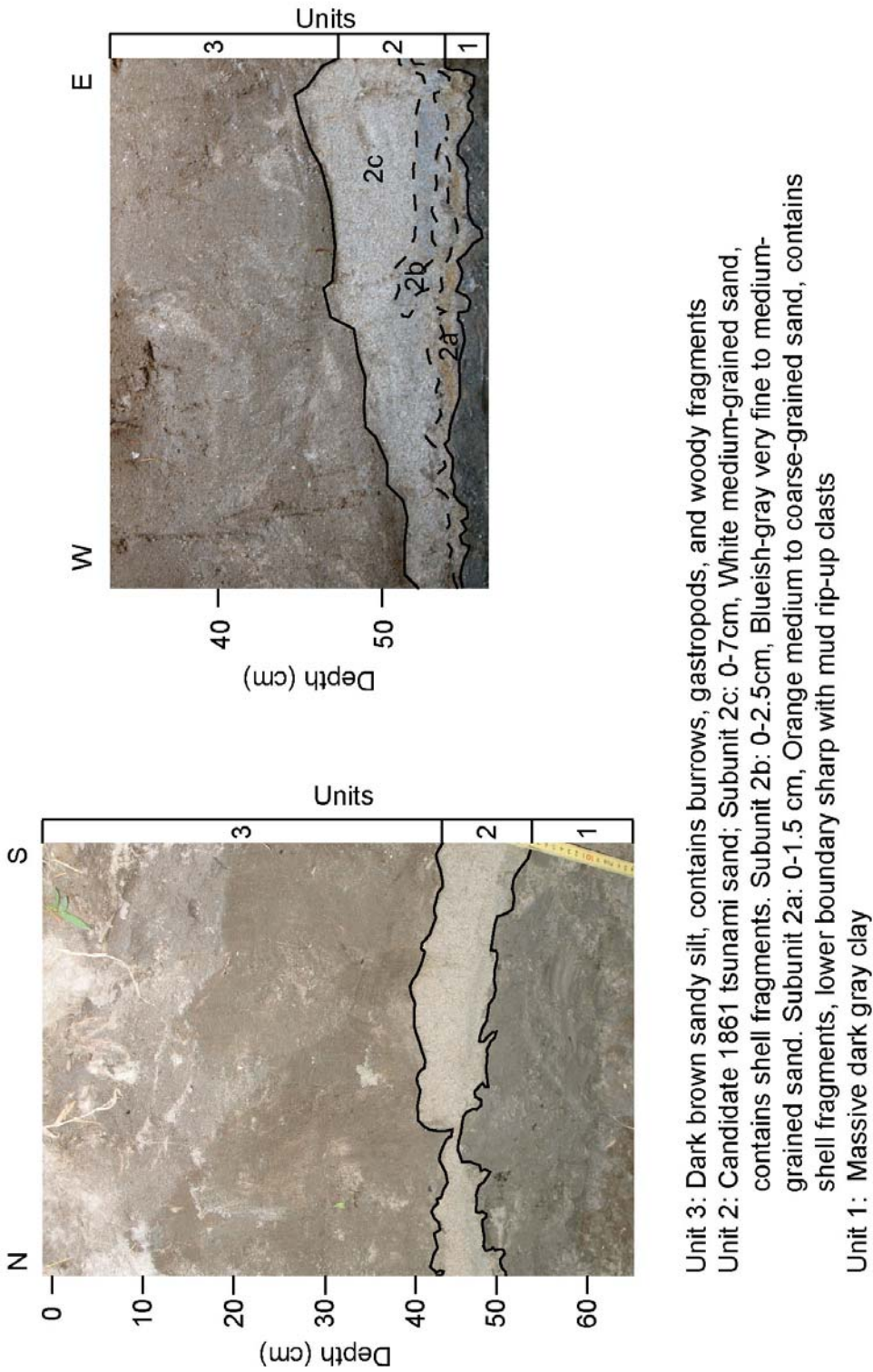


Figure 11. Inor trench F stratigraphy (see Figure 4 for trench location).

the ground surface at trench E prior to the 2004 tsunami. Another possibility for sand thickness variations is that the sand was eroded in trenches B and D by backwash during the 2004 tsunami. Typically, tsunami return flows follow topographic lows (Morton *et al.*, 2007), such as the Inor River.

#### *Grain Size Analyses*

Grain size analyses aided in the classification of the candidate 1861 tsunami sand. Grain size analyses were completed, by Shige Fujino at Kyoto University, Japan, on the beach sand at Inor and trench wall exposures containing candidate tsunami sands. A 1cm-wide vertical sample was collected from each sand layer within the trench wall exposures (Figure 12).

The grain size analyses used methods described by Minoura *et al.* (1988) (Figure 13). The grain size analysis method determines the settling velocity of particles by timing how long particles take to move through a column of water at a specified temperature (Boggs, 2001). The particle size is evaluated using the logarithmic scale phi,  $\Phi$  (Krumbein, 1934), by the following equation:

$$\Phi = -\log_2 d = -[(\log_{10} d) \div (\log_{10} 2)] \quad (1)$$

where  $d$  is the grain diameter in millimeters. The particle size is evaluated using the phi scale because it is easier to analyze statistically. Prior to placing the samples into the settling tube, the dried samples were weighed ( $w1$ ). Silt to clay-sized particles ( $\Phi > 4$ ) were removed from the sample using a mesh screen. Next, the dried sample, void of silt to clay-sized particles, was re-weighed ( $w2$ ). Finally, a mud ratio, which determines the

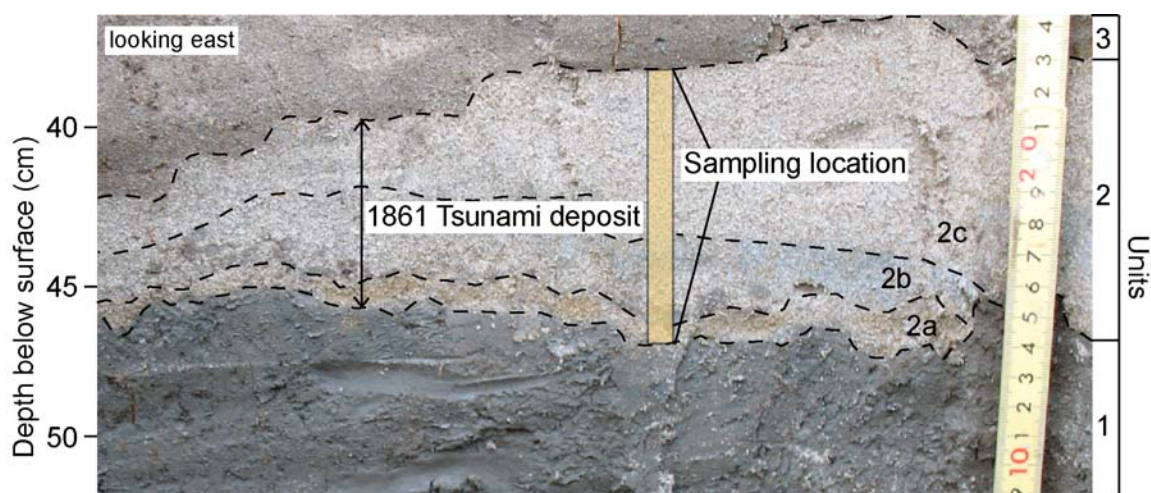


Figure 12. Sample location for grain size analysis of the candidate 1861 tsunami deposit, trench F, Inor.

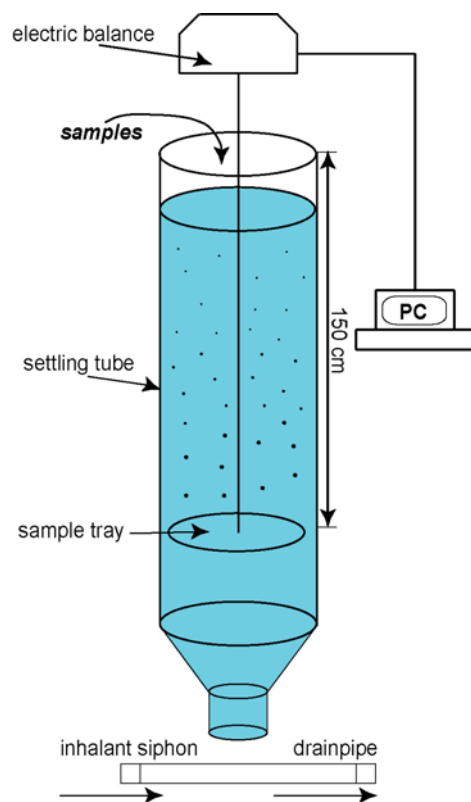


Figure 13. A schematic diagram of a settling tube.

ratio of silt to clay-sized particles with respect to larger grains in the original collected sample, was calculated using the following equation:

$$\text{mud ratio} = \frac{(w_1 - w_2)}{w_1} \times 100 \quad (2)$$

The sample was then placed into the 150cm-long settling tube filled with 20°C water.

The grain size measurement ranged from 0 to 4 phi, which includes grain sizes from very coarse sand (2.0mm diameter) to very fine sand (1/16mm diameter), respectively.

Grain size analyses were completed at Inor to determine whether the candidate 1861 tsunami sands within trench wall exposures (A, B, D, E, F, and I) matched the grain size of the sand from the nearby beach (Figures 14 and 15). In addition, we compared deposits stratigraphically below the tsunami sand, unit 1, with candidate 1861 tsunami sand, unit 2. These deposits included unit 1, a blue to gray clay from trench E and a gray to blue silt from trench L, which are perhaps correlative units (Figure 16). In trench D, 5 horizontal sand samples from 5 sub-layers within the candidate tsunami sand were collected in order to document sedimentary structures (e.g., graded bedding) and grain size variation from the base of the deposit to the top (Figure 17). Sands other than tsunami sands, such as parallel laminated sand from exposures in trench L and a cross-stratified sand from trench J exposures were also analyzed and compared to the candidate tsunami sand (Figure 16).

In trench B, the 1861 tsunami sand (unit 2) coarsens upwards, from 3.295 Φ at the base of the sand to 2.864 Φ at the top of the sand deposit (Figure 14). The 1861 tsunami sand in trench B contains two subunits, 2a and 2b (Figure 7), possibly the result of two

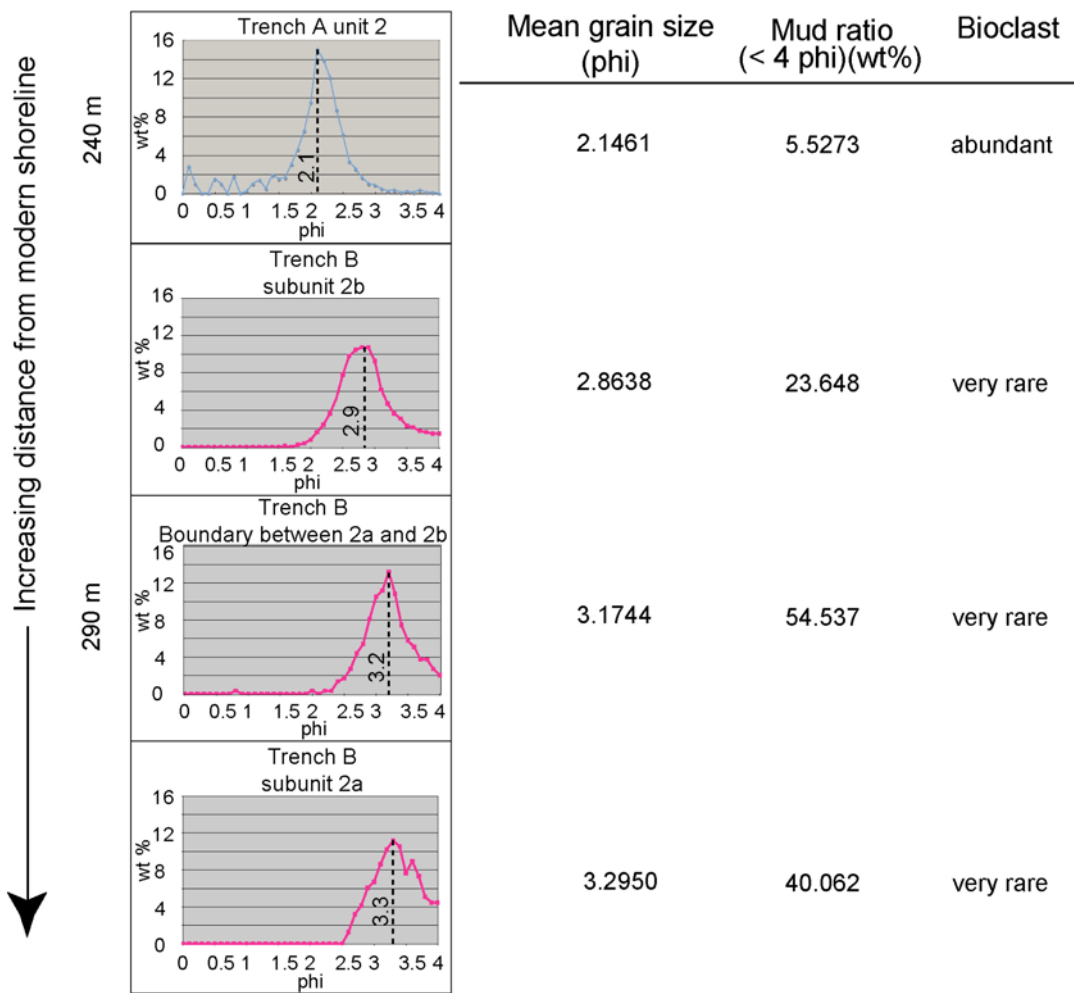


Figure 14. Graphical analyses (weight percent versus phi) and statistics of the candidate 1861 tsunami sand in Inor trenches A and B; trench A (blue graph) shows graphical analysis of entire candidate tsunami sand sample (see Figure 5 for stratigraphy); trench B (pink graphs) show graphical analyses and statistics from subunits 2a, 2b, and the thin mud layer separating subunits 2a and 2b (see Figure 6 for stratigraphy); dashed line on graphs is the mean grain size in phi units; see Figure 4 for trench locations.

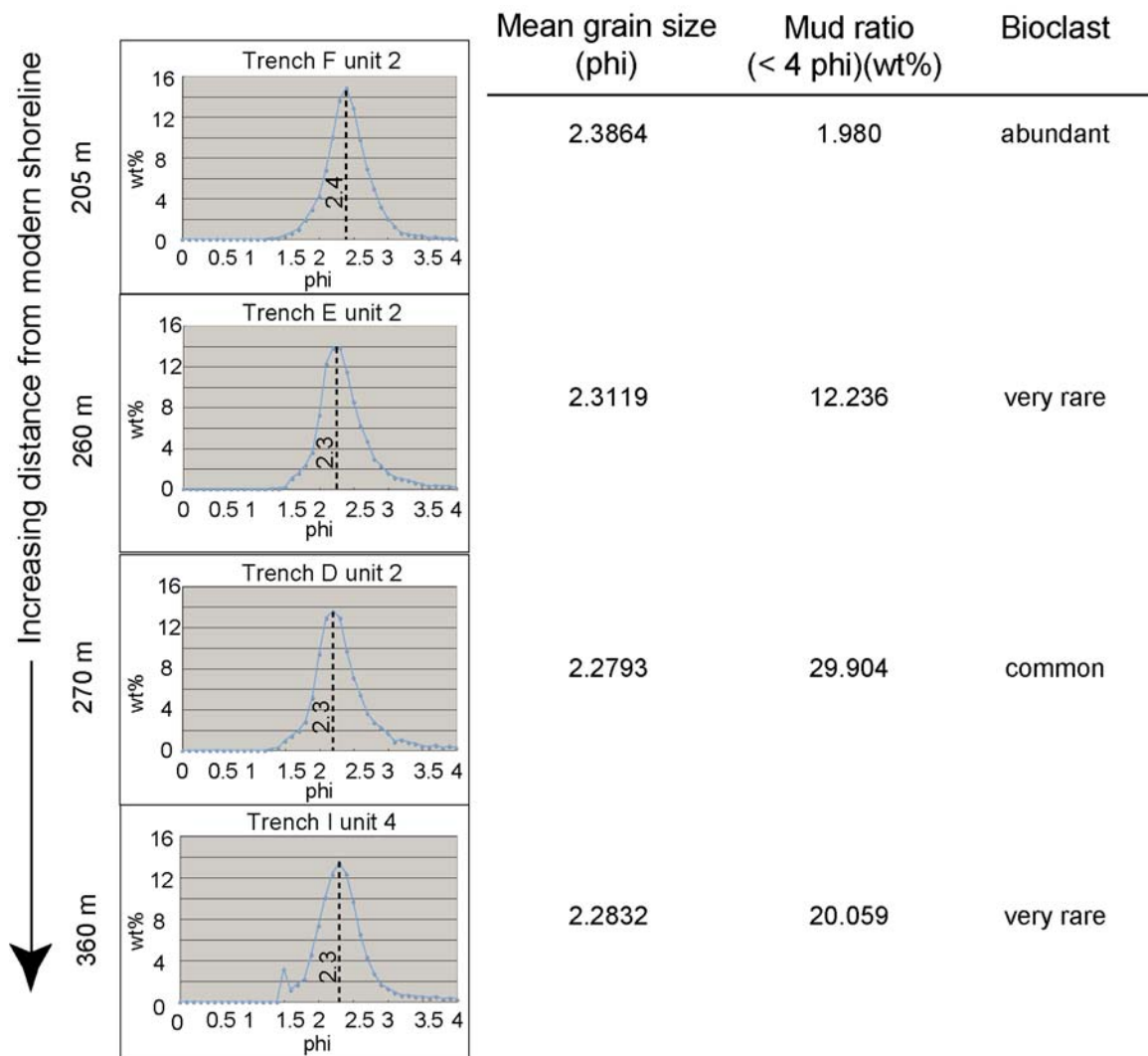


Figure 15. Graphical analyses (weight percent versus phi) and statistics of the candidate 1861 tsunami sand in Inor trenches F, E, D, and I; dashed line on graphs is the mean grain size in phi units; see Figure 4 for trench locations.

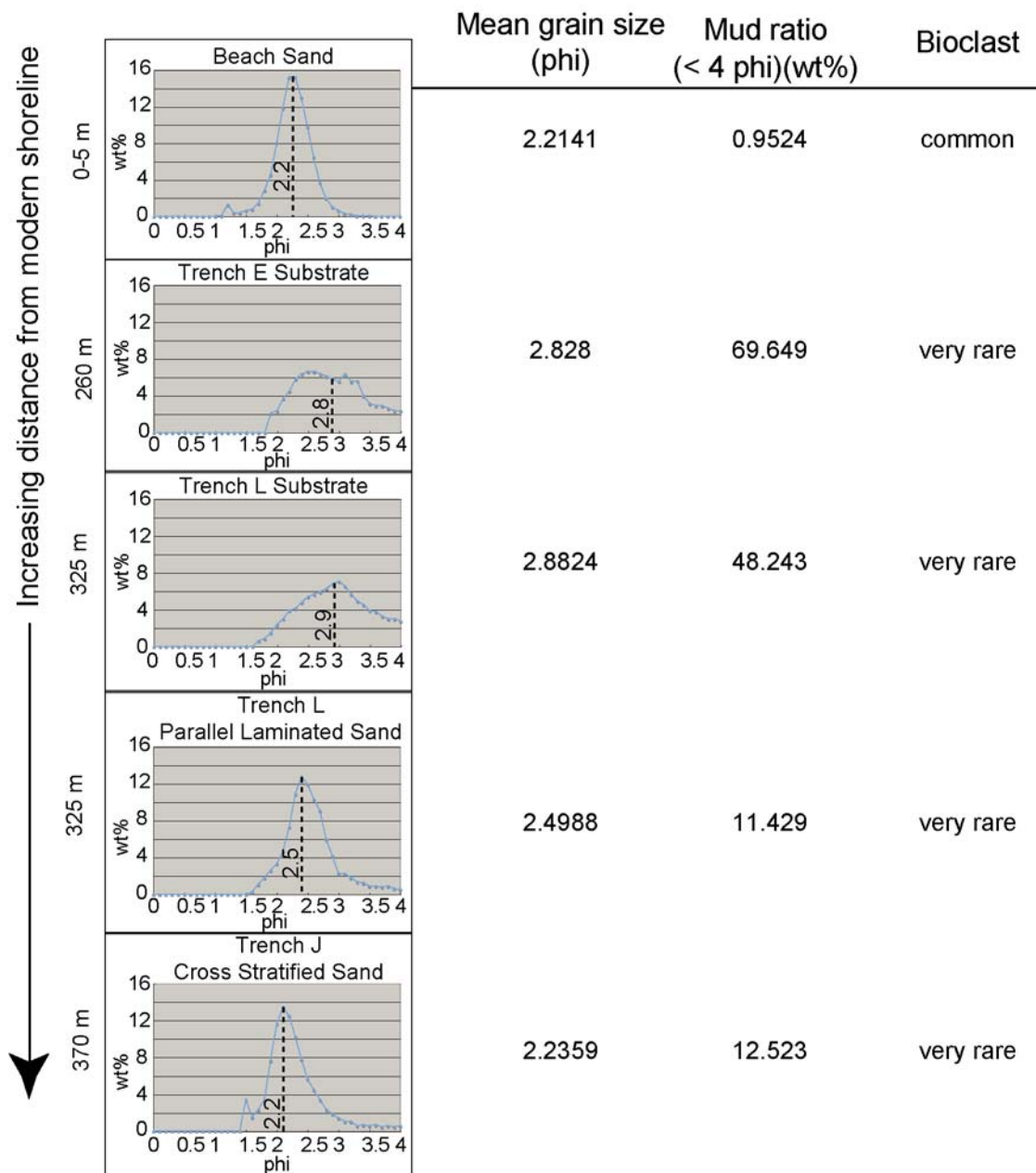


Figure 16. Graphical analyses (weight percent versus phi) and statistics of modern beach sand at Inor, substrate material (unit directly below the candidate 1861 tsunami sand) from trenches E and L, parallel laminated sand from trench L, and cross-stratified sand from trench J; dashed line on graphs is the mean grain size in phi units; see Figure 4 for trench locations.

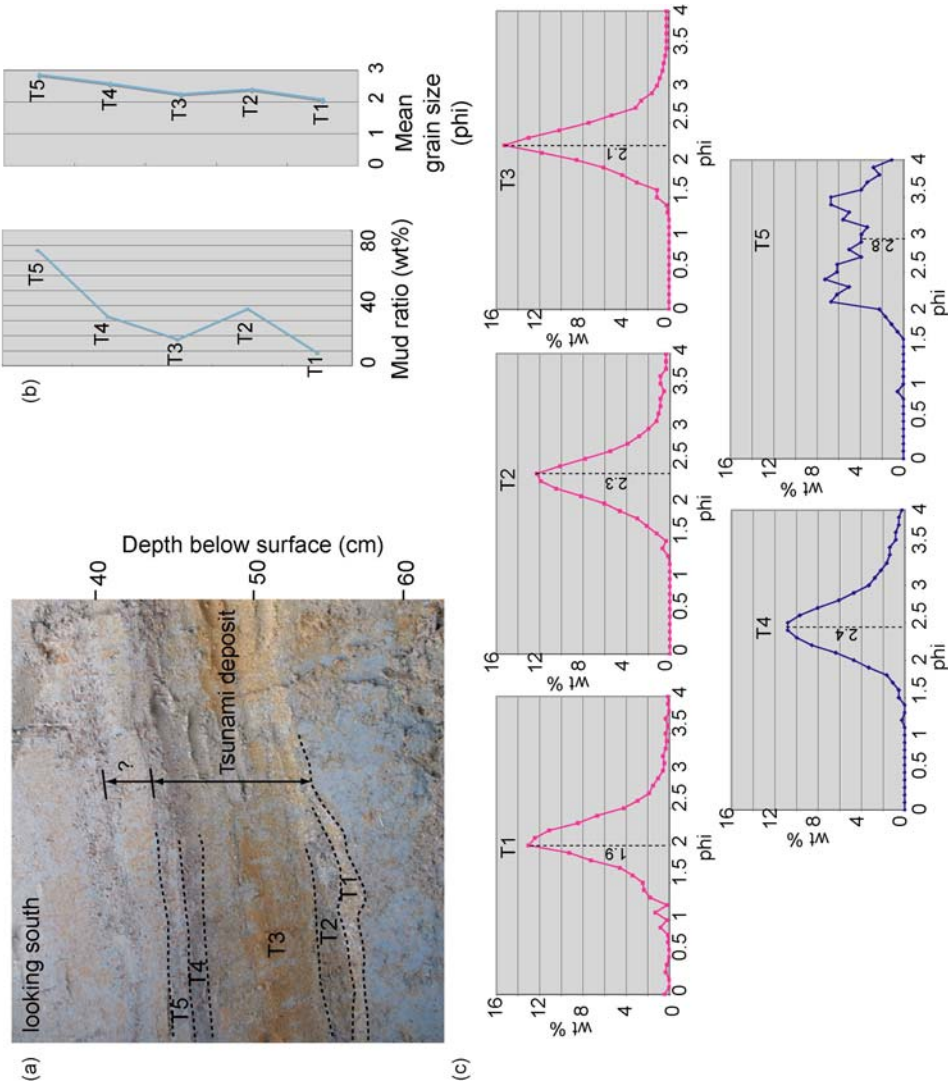


Figure 17. Grain size analysis of Inor trench D. (a) Subunits within trench wall exposure. (b) Mud ratio and mean grain size of subunits T1 through T5. (c) Weight percent versus phi for grain sizes of sub-layers T1 through T5; sub-layers T1 through T3 (pink graphs) represent candidate 1861 tsunami sand layers, sub-layers T4 and T5 (blue graphs) are uncertain candidate 1861 tsunami sand layers; dashed line is the mean grain size in phi units; see Figure 4 for trench location.

consecutive waves. Reverse grading of subunits 2a and 2b perhaps indicate a stronger second wave in the wave train. Most 2004 tsunami deposits near Banda Aceh were normally graded, although reverse grading was also found within individual units (Moore *et al.*, 2006).

The mud ratio (Figures 14, 15, and 16) is the weight percent of the silt-and clay-sized particles with respect to the entire collected sample. The mud ratio is calculated prior to the removal of silt and clay sized particles from the original sample. The boundary between subunits 2a and 2b in trench B resulted in a mud ratio of 54.54 percent, possibly representing a break between two sequential waves (Figure 14). The high mud ratio may be from a decrease in wave velocity during backwash of the first tsunami wave. For example, the  $M_w$  7.0 1998 Papua New Guinea and the  $M_w$  8.4 2001 Peru tsunami deposits contain from one to three sub-layers that are normally graded (Morton *et al.*, 2007). Eyewitnesses of the Papua New Guinea tsunami said there were three waves and the 2001 Peru tsunami produced three to four waves (Morton *et al.*, 2007). Although each sub-layer may represent a separate wave, this is difficult to demonstrate since wave interference from sequential backwash and run-up can affect deposition (Morton *et al.*, 2007).

Numerous studies show that tsunami deposits fine landward, from a decrease in the flow velocity of tsunami waves (Minoura *et al.*, 1996; Benson *et al.*, 1997; Moore *et al.*, 2006; Morton *et al.*, 2007). The candidate 1861 tsunami sand decreases in grain size inland at Inor from trench A to trench B (Figures 4 and 14). Similarly, moving inland from trench F to E to I (Figure 4), the mean grain size is relatively similar, but the mud

ratio increases significantly (Figure 15). The increasing mud ratio indicates a landward fining trend.

Five sub-layers from trench D at Inor were analyzed to determine variations in mud content and mean grain size (Figure 17). Trench D fines upward from a mean grain size of 1.9  $\Phi$  at the lowest sub-layer T1, to 2.8  $\Phi$  at the uppermost sub-layer, T5 (Figure 17). The fining upward sequence exposed in trench D is similar to other tsunami deposits. For example, fining upwards sand units were documented in tsunami deposits on Vancouver Island, British Columbia from the 1964  $M_w$  9.2 Alaskan earthquake (Benson *et al.*, 1997). Here, the sand fines upwards from a decrease in flow velocity. Although the mud ratio in trench D increases from sub-layer T1 to T5, the mud ratio increases from T1 to T2, then decreases from T2 to T3 (Figure 17). This might represent consecutive waves. Mud content increases during backwash, when flow velocities are also lower than during run-up. While sub-layers T1 through T4 have distinct mean grain sizes, sub-layer T5 is very poorly sorted, including grain sizes from 2.0  $\Phi$  to 4.0  $\Phi$  and a mud ratio of about 70 percent. This data indicates that sub-layer T5 may be a part of the overlying sandy silt unit (Figure 8).

Unit 2 in trenches J and L corresponds to a parallel-laminated and cross-stratified sands from trenches, respectively, and are most likely river-derived. Parallel lamination and cross-stratification are common facies in fluvial channels (Reading, 1996) and form under medium flow velocities (Boggs, 2001). The cross-stratified sand from trench J dips eastward and away from the Inor River, implying deposition from a flood event. Although cross-stratified and parallel laminated sands have been observed in tsunami

deposits (Moore *et al.*, 2006) and the grain size of these sands from trenches J and L at Inor are similar to the candidate 1861 tsunami sand (Figure 16), the lack of bioclastic material in trenches J and L makes it difficult to verify these sands as tsunami-derived.

Many tsunami sand studies show that the grain size distribution from modern beach sand matches that of tsunami sand deposits inland from the shoreline (Morton *et al.*, 2007; Moore *et al.*, 2006; Minoura *et al.*, 1996). The grain size distributions of the candidate 1861 tsunami sands from trenches at Inor (Figures 14 and 15) are analogous to the modern beach sand (Figure 16). The mud ratio of the beach sand is 0.95 percent. The mud ratio of unit 2 sands from exposures in trenches A, B, D, E, F, and I is higher than that of the beach sand. Here, the tsunami most likely scoured finer grained sediments as it moved inland and deposited these along with the beach sand. Calcareous materials such as algae and/or bivalves are present in both the sand collected directly from the modern beach and in candidate tsunami sands from the walls of trenches A, B, D, and F, suggesting a shallow marine or beach origin.

#### *Busong Bay*

Busong Bay was targeted in order to characterize tsunami inundation in a bay environment and to document any lateral variations of the sedimentology of candidate tsunami sands among different excavations (Figure 18). Five excavations parallel to the beach were made about 50 m inland (Figure 18). The stratigraphy was described in detail and samples were collected for U–Th geochronology.

Five stratigraphic units were identified in trench wall exposures at Busong Bay (Figure 19). Unit 1, the stratigraphic base, consists of gray fine-grained sand and was

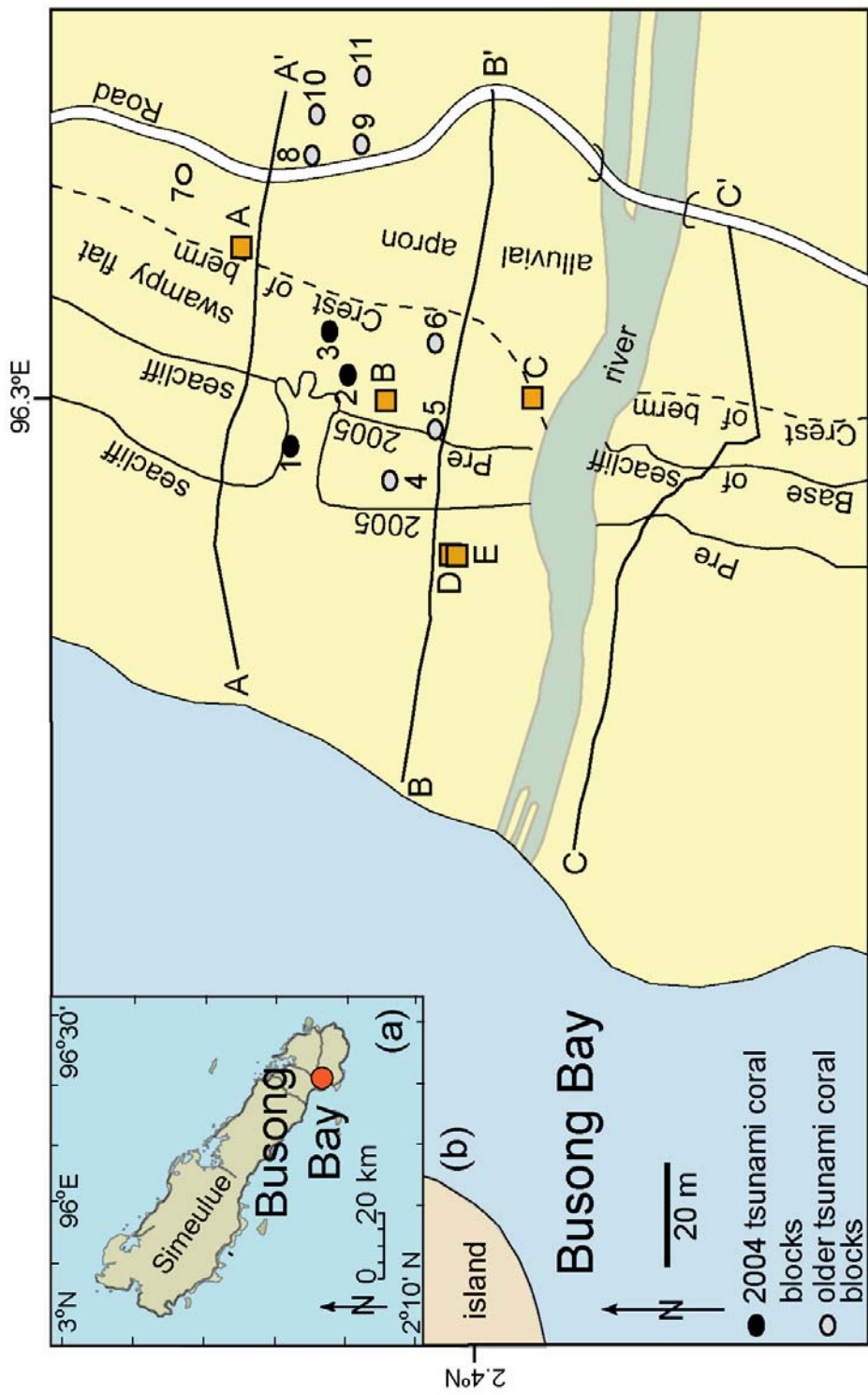


Figure 18. Geomorphology of Busong Bay; solid black circles, coral boulders from the 2004 tsunami; open circles, coral boulders from an older tsunami.



Unit 5: Candidate 2004 and 2005 tsunami sands, subunit 5f is the 2005 tsunami sand, subunits 5a through 5e are 2004 tsunami sands; Subunit 5a: 4-10 cm, fine to silty sand. All subunits have a color change from gray to white moving stratigraphically upwards and fine upwards. Subunit 5b: 3-4 cm, medium to fine sand. Subunit 5c: 2-3 cm, medium sandy silt. Subunit 5d: 2-3 cm, fine sand, massive. Subunit 5e: 4-5 cm, medium sand with weak laminations, capped with organic-rich layer. Subunit 5f: 4-5 cm, medium sand, massive.  
 Unit 4: Dark brown peat layer with some silty sand, lower boundary contains coral fragments 5cm in length, many roots, some gastropods  
 Unit 3: 1861 tsunami sand: white to gray very fine to medium sand, algae fragments at the top and bottom of unit, fines upwards  
 Unit 2: Dark brown peat layer with some silty sand, lower boundary contains coral fragments mixed with sand and mud, some roots and gastropods  
 Unit 1: Gray fine grained sand, coarsens upwards, root at the top of unit, contains bioturbation

Figure 19. Busong Bay trench A stratigraphy (see Figure 18 for trench location).

likely the old beach surface. Unit 2, a dark brown peat layer, overlies unit 1. The peat layer most likely formed in a restricted tidal flat setting, reflected in the present geomorphology as a tidal swamp (Figure 18). Tidal flats commonly form behind

seacliffs, which act as a barrier from waves and tides (Woodroffe, 2003). Gastropods and coral fragments up to 5cm in diameter were found within trench wall exposures at Busong Bay (Figure 19). The gastropods may have been deposited from the river during a flood episode. The coral fragments at the lower boundary of the peat layer (Figure 19) were probably eroded from the adjacent beach cliff to be deposited on the swampy flat (Figure 18).

Unit 3 is a white to gray very fine to medium sand and represents the candidate 1861 tsunami sand. Unit 3 is bracketed by peat (units 2 and 4). Algae and coral fragments within unit 3 imply a marine origin. Unit 4, like unit 2, is a dark brown peat layer that contains some silty sand.

The 2004 tsunami sand, unit 5, caps the stratigraphic sequence (Figure 19). The 2004 tsunami sand is defined by five subunits, 5a through 5e (Figure 19). This unit fines upwards, a common feature observed in tsunami deposits (Minoura *et al.*, 1996; Benson *et al.*, 1997; Moore *et al.*, 2006; Morton *et al.*, 2007). The 2004 tsunami sand subunit 5b contains flame structures at its base (Figure 19). Flame structures form from a less dense, water-saturated substrate material (i.e., subunit 5a sand) that is squeezed upward through the overlying sand layer (Boggs, 2003). An organic-rich layer caps the 2004 tsunami sand, separating the 2004 sand from the 2005 tsunami sand. In the three months between the December 26, 2004 and March 28, 2005 earthquakes, grass began to grow on top of the 2004 tsunami sand, forming an organic-rich layer.

Coral boulders have been deposited on the ground surface at Busong Bay from the 2004 tsunami and at least one older event, possibly the 1861 tsunami (Figure 18).

Table 2  
Busong Bay Tsunami-Derived Coral Boulders

| Coral boulder | Diameter<br>(m) | Distance from<br>Modern shoreline<br>(m) | 2004 tsunami<br>deposit | Older tsunami<br>deposit |
|---------------|-----------------|--|-------------------------|--------------------------|
| 1             | 5.0             | 50                                       | X                       |                          |
| 2             | 1.5             | 65                                       | X                       |                          |
| 3             | 1.7             | 75                                       | X                       |                          |
| 4             | 2.5             | 52                                       |                         | X                        |
| 5             | 7.0             | 63                                       |                         | X                        |
| 6             | 4.0             | 80                                       |                         | X                        |
| 7             | 3.5             | 95                                       |                         | X                        |
| 8             | —               | 105                                      |                         | X                        |
| 9             | —               | 116                                      |                         | X                        |
| 10            | —               | 118                                      |                         | X                        |
| 11            | —               | 125                                      |                         | X                        |

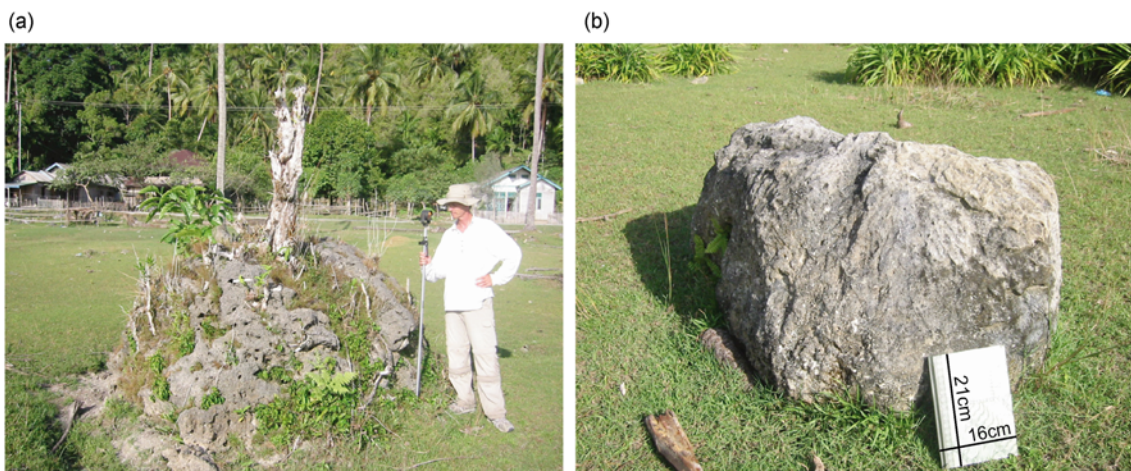


Figure 20. Busong Bay coral boulder tsunami deposits. (a) Coral boulder deposited from an older tsunami, 80 m inland from shore; reflector is 1.5 m in height. (b) Coral boulder deposited by the 2004 tsunami, 50 m from shore; notebook for scale.

The coral boulders deposited from the 2004 tsunami are found up to 75m inland from the modern shoreline and are up to 5m in diameter (Table 2). The 2004 boulders lack signs of weathering, are angular, and lie directly on the modern ground surface (Figure 20).

The older coral boulders are found up to 125m inland from the modern shoreline and are up to 7m in diameter (Table 2). The older boulders are weathered, rounded, have vegetation growing on them, and are buried beneath the modern ground surface (Figure 20). The modern shoreline of Busong Bay lacks coral growth. Therefore, the 2004 and older coral boulders are likely from the nearby island composed of coral that underwent coseismic uplift during the 2004 earthquake (Figure 18).

The geomorphology at Busong Bay is similar to that of a beach-ridge strandplain (Figure 18), a wave-dominated, sand-rich shoreline (Reading, 1997). The nearby rivers and the shelf provide a source for the beach ridge sand (Reading, 1997). Long-shore drift distributes the sand along the coast that forms the beach ridges (Reading, 1997). Beach ridges commonly form as a response to falling sea level (Woodroffe, 2003). Survey profiles at Busong Bay show up to three beach ridges that gradually dip seaward, probably the result of local uplift. Simeulue Island has undergone local sea-level fall in response to uplift (Briggs *et al.*, 2006), which is reflected in the geomorphology at Busong Bay.

#### *Langi Bay*

Langi Bay is a restricted bay with very fine-grained sand and mud exposed near the shore (Figure 21). Five excavations across the trace of the modern terrace were made to show lateral variations in the coastal stratigraphy (Figure 21). The stratigraphy was described in detail and samples were collected from trench wall exposures for AMS analyses.

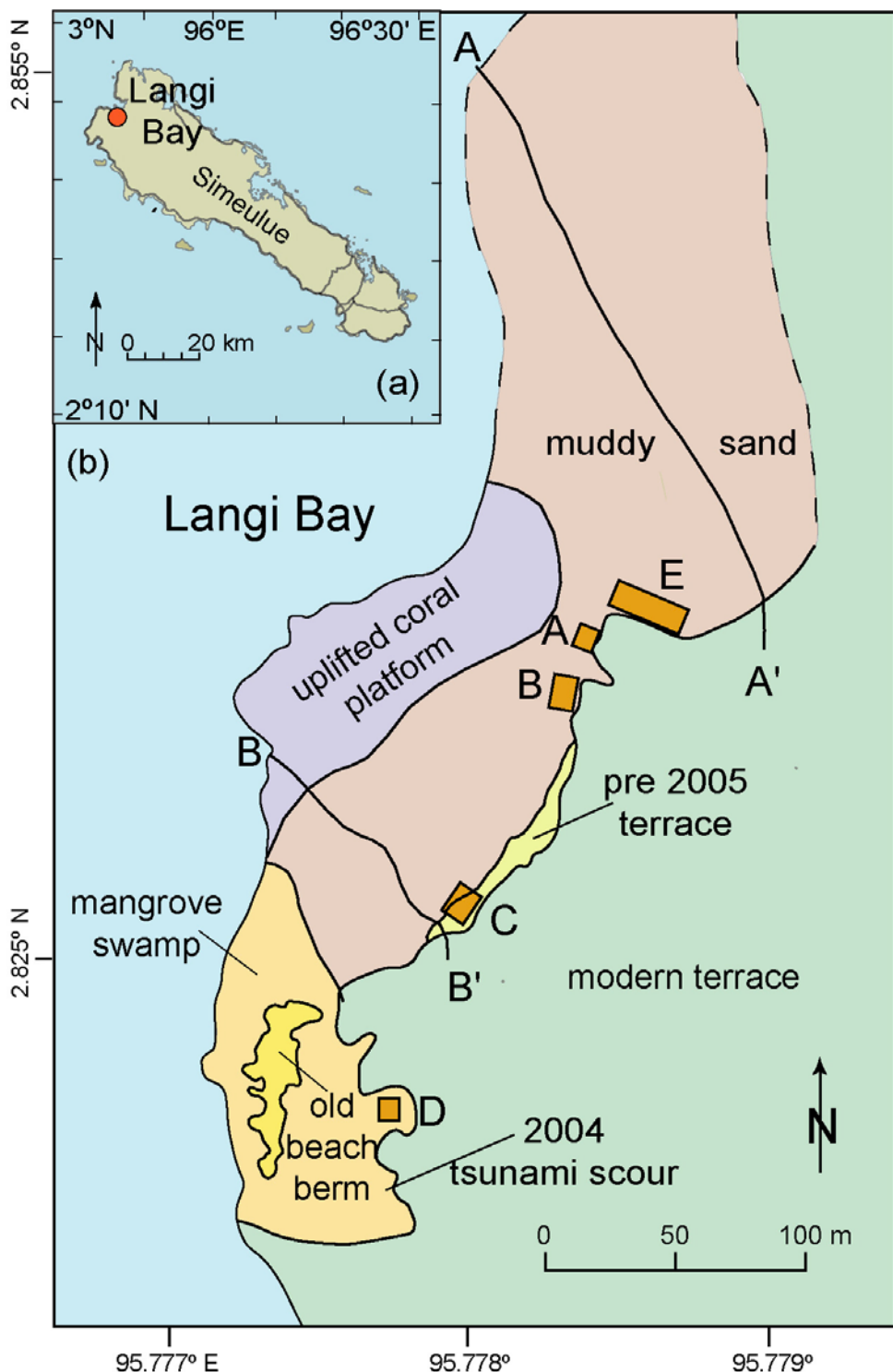
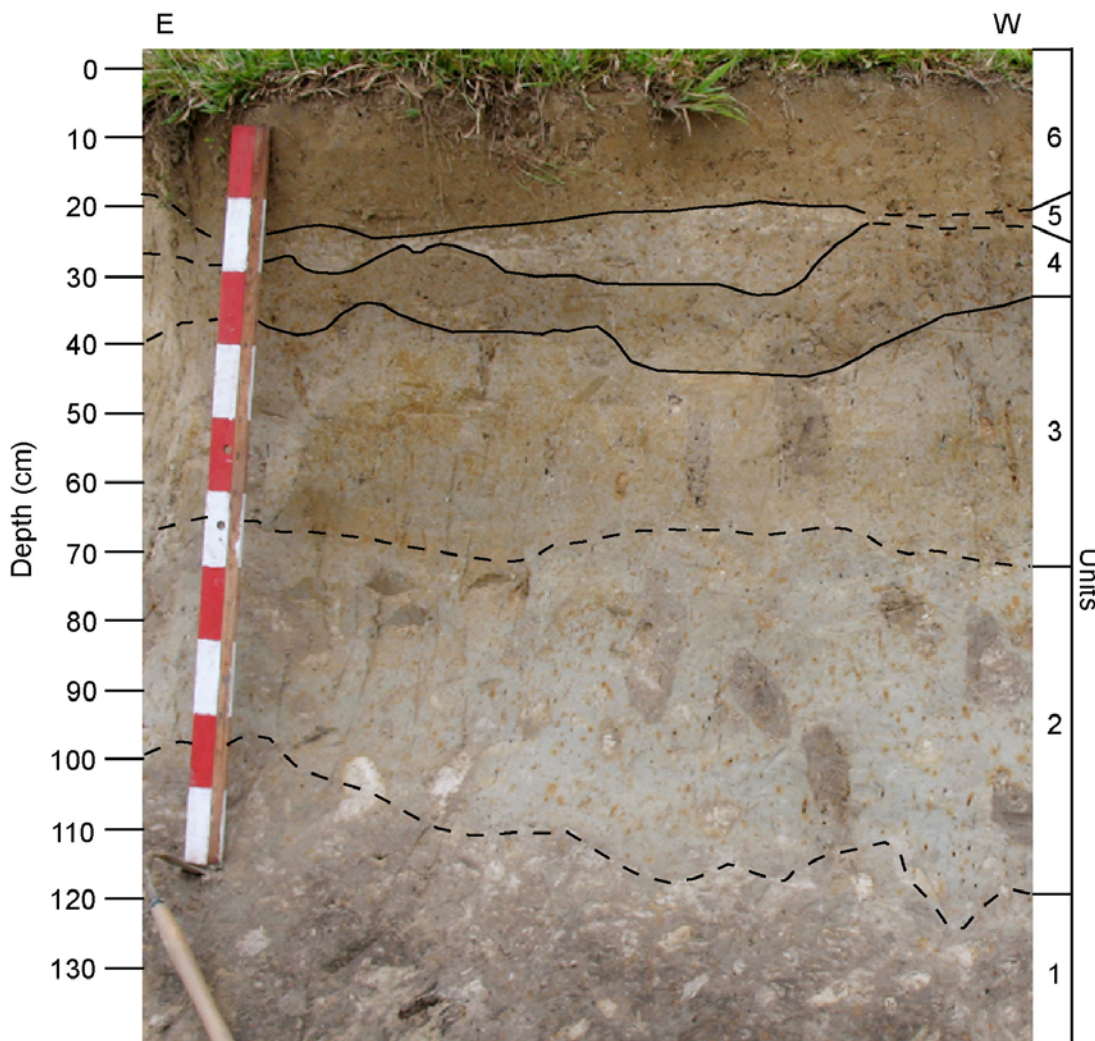


Figure 21. Geomorphology of Langi Bay. (a) Location of Langi Bay on Simeulue Island. (b) Langi Bay geomorphology.

Four major stratigraphic units define Langi Bay. The first is the stratigraphic base, unit 1, which is a massive dark gray to black organic-rich silty sand. In trench E, this unit is 90 cm thick and is represented by units 1-3 (Figure 22) and by unit 1 in trench A (Figure 23). This unit undergoes a color change from black to blue-gray. Throughout unit 1, there are oxidized roots and bioturbation. Oxidation occurs during exposure to the atmosphere (Reading, 1997). The roots were probably oxidized during low tide when this unit was at the surface. The gray color in unit 1 indicates a water-laden environment (Reading, 1997) and was likely deposited in a quiet water setting, perhaps a tidal marsh. A mangrove swamp is currently near the shoreline (Figure 21). Mangrove trees, which are halophytic (salt-tolerant), typically grow in upper-intertidal environments (Woodroffe, 2003). Extensive bioturbation is common in unit 1, similar to a modern mangrove swamp with a rich diversity of flora and fauna.

The second major unit is a white fine to medium-grained sand. This unit is represented by unit 5 in trench E (Figure 22) and unit 2 in trench A (Figure 23). This sand unit is a candidate 1861 tsunami sand. In trench A, unit 2 is defined by two subunits (2a and 2b) that fine upwards (Figure 23). The subunits may represent two consecutive waves within the tsunami wave train.

Third, a light brown silt brackets the candidate 1861 tsunami sand in trench E (units 4 and 6; Figure 22) and overlies the sand in trench A (unit 3; Figure 23). In trench wall exposures A and E, this unit consists of massive silt, due to extensive bioturbation from roots (Figures 22 and 23). This unit forms the modern beach terrace



- Unit 6: Brown peat, grades down to massive brown-blue bioturbated, sandy silt
- Unit 5: Candidate 1861 tsunami sand; White fine sand, bioturbated, sharp lower boundary
- Unit 4: Light brown to blue-gray silt to very fine sand, lots of roots and burrows, oxidized, gradual lower boundary
- Unit 3: Light gray to blue very fine sand, burrows up to 6 cm in length, lots of roots, gradual upper and lower boundaries
- Unit 2: Blue-turquoise very fine to fine sand, large burrows (5-7 cm wide by 20 cm long), oxidized roots, massive
- Unit 1: Black to dark gray very fine to medium sand to silt, very poorly sorted, organic content increases downwards, contains oxidized roots.

Figure 22. Langi Bay trench E stratigraphy (see Figure 21 for trench location).

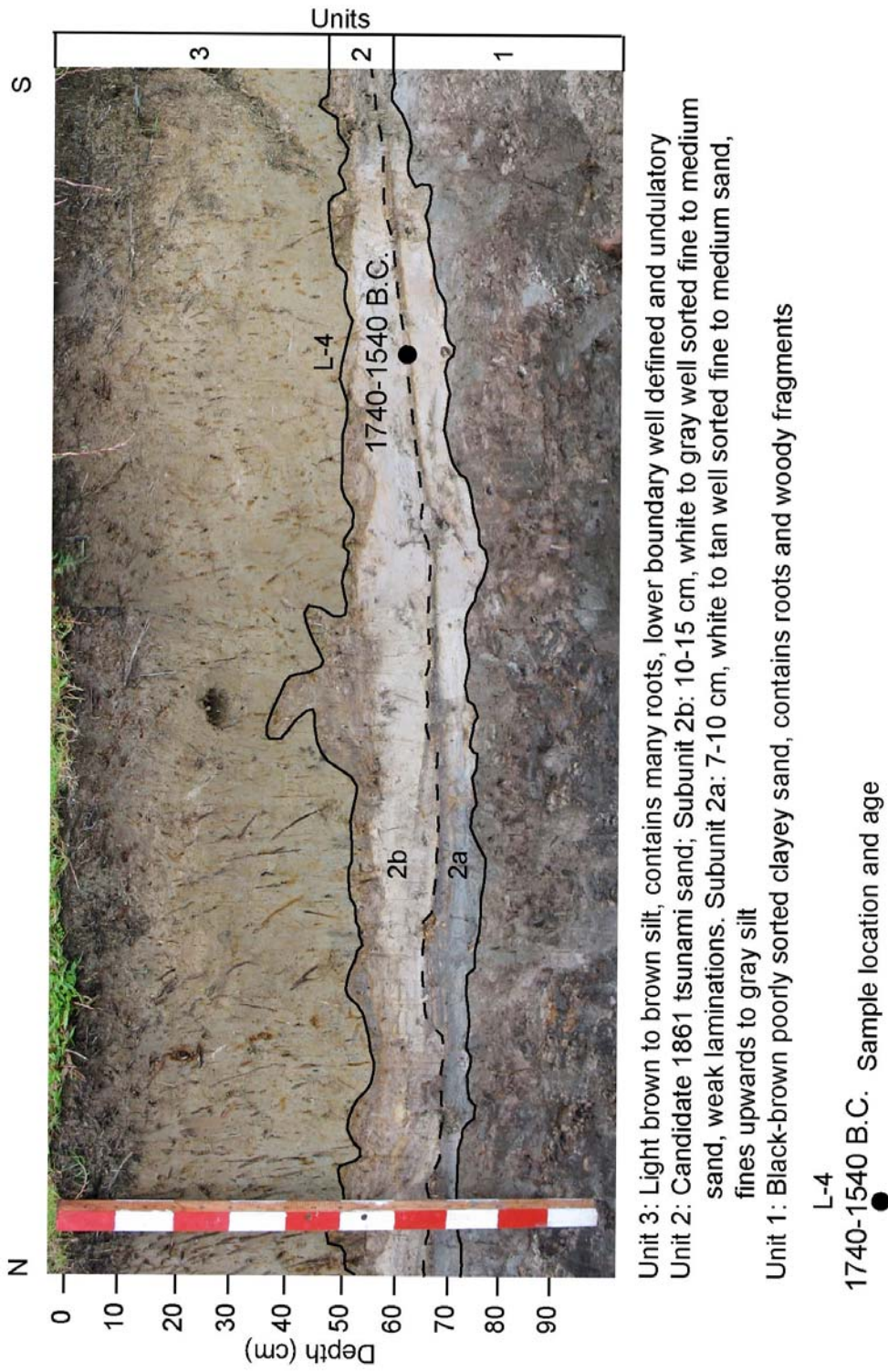


Figure 23. Langi Bay trench A stratigraphy (see Figure 21 for trench location).

(Figure 21). In trench D, this unit is gray and corresponds to unit 1 (Figure 24). Trench D is in a topographic low and mangrove forest, and is therefore underwater during high tide, resulting in the gray color.

The final major stratigraphic unit at Langi Bay is the candidate 2004 tsunami sand (Figure 24). This very fine to fine white to gray sand is represented by unit 3 in trench D (Figure 24) and is not present in the other excavations at Langi Bay. Unit 3 consists of three undulating fining upwards layers. Based on the multiple fining upwards sequences, unit 3 represents deposition from consecutive waves. This sand unit is thought to be 2004 based on the plastic rip-up clasts at the base of the unit (Figure 24). The stratigraphic units in trench D at Langi Bay likely correlate above the units in trenches A and E (Figure 25).

### Geochronology

#### *Accelerator Mass Spectrometry Radiocarbon Dating*

Accelerator Mass Spectrometry (AMS) was used to constrain the age of stratigraphic layers using detrital charcoal, peat, and wood fragments. AMS radiocarbon dating was completed at the Institute of Accelerator Analysis, Ltd. in Shirakawa City, Fukushima, Japan. Wood fragments and gastropods were collected from trench wall exposures at Inor and Langi Bay (trench A).

At Inor, a unit 1 wood fragment 13-15 cm below unit 2, the candidate 1861 tsunami sand, yielded a calibrated age range of 310 years B.P. to modern (Figure 6 and Table 3). Gastropods from unit 3 were collected in order to bracket the age of tsunami



Unit 3: Candidate 2004 tsunami sand; very fine white to gray sand, contains minor laminations. Organic content and bioturbation increase downward, contains plastic rip-up clasts

Unit 2: Massive very fine to fine gray sand with burrows

Unit 1: Fine white to brown peaty sand intercalated with black silty sand, contains organic material

Figure 24. Langi Bay trench D (see Figure 21 for trench location).

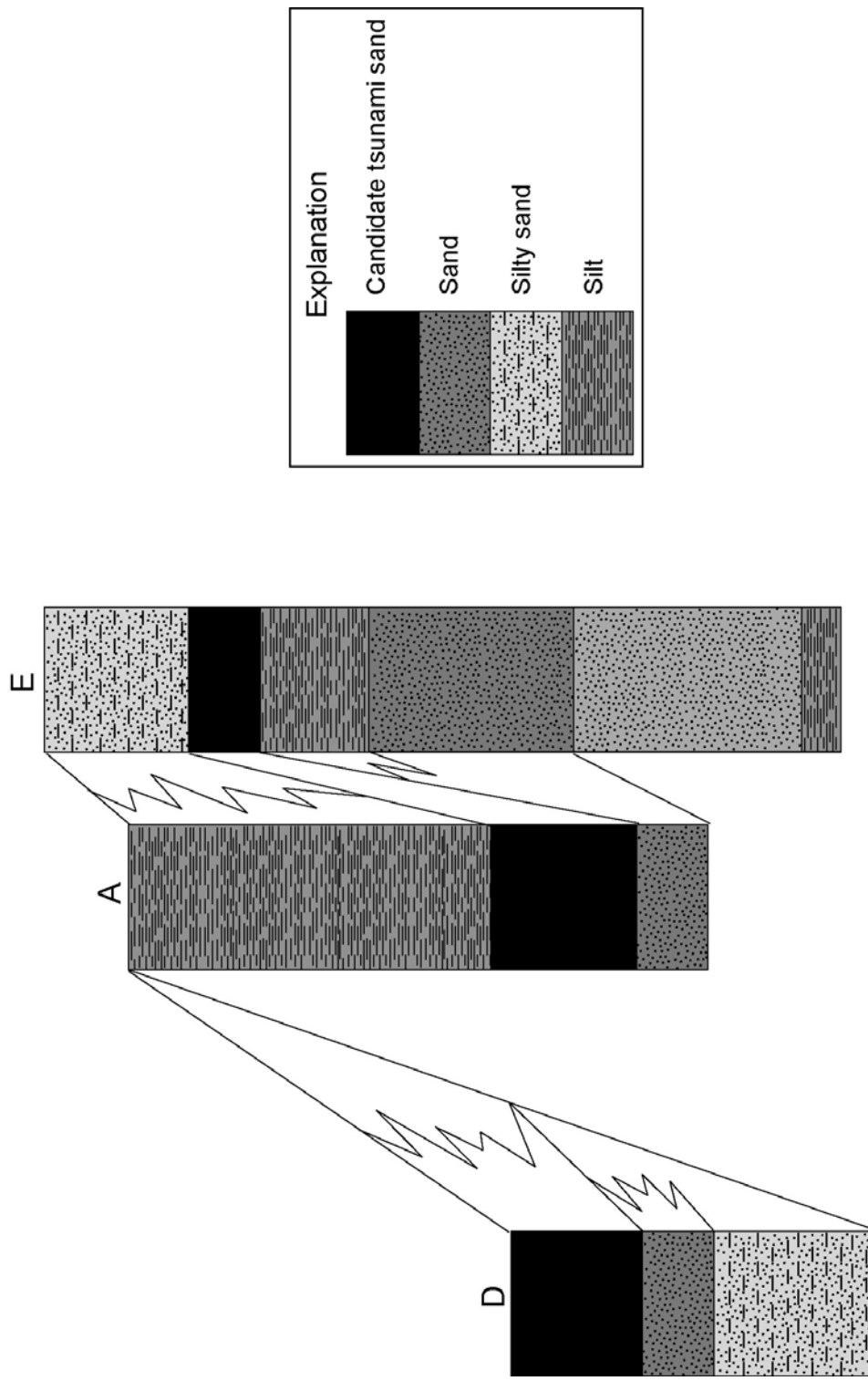


Figure 25. Langi Bay fence diagram of trenches D, A, and E (see Figure 21 for trench locations).

*Table 3*  
Radiocarbon Analyses

| Sample Number * | Laboratory Number <sup>‡</sup> | $\Delta^{14}\text{C}$ (p. mil) <sup>†</sup> | $^{14}\text{C}$ Age <sup>§</sup><br>(Years B.P.) <sup>¶</sup> | Calibrated Age Range<br>(Years B.P.) <sup>¶</sup> | Location, Trench and<br>Stratigraphic Unit <sup>#</sup> | Depth Below<br>Ground Surface<br>(cm) |
|-----------------|--------------------------------|---|---|---|---|---------------------------------------|
| I-1             | IAAA-70391                     | $370.7 \pm 4.9$                             | Modern  | Modern  | Inor, trench A<br>unit 3                                | 39–41                                 |
| I-2             | IAAA-70390                     | $228.7 \pm 4.3$                             | Modern  | Modern  | Inor, trench A<br>unit 3                                | 41–43                                 |
| I-3             | IAAA-70389                     | $-10.7 \pm 3.7$                             | $90 \pm 30$   | 310–Modern  | Inor, trench A<br>unit 1                                | 52–54                                 |
| I-4             | IAAA-70388                     | $-335.8 \pm 3.0$                            | $3290 \pm 40$   | 3690–3490   | Langi Bay, trench A<br>unit 2                           | 62–64                                 |

\*Samples are listed in relative stratigraphic order from top to bottom for Inor, trench A.

<sup>†</sup>  $\Delta^{14}\text{C}$  (ppm), ratio of  $^{14}\text{C}/^{12}\text{C}$ .

<sup>‡</sup> Samples were prepared and run at Institute of Accelerator Analysis Ltd., Fukushima, Japan.

<sup>§</sup> The reported  $^{14}\text{C}$  ages use Libby's half-life of 5568 years according to Stuiver and Polach (1977); analytical uncertainties shown are 1 standard deviation.

<sup>¶</sup> The calibrated calendar ages were found using Oxcal v.3.10 (Bronk Ramsey, 2005) and normalized to 2 standard deviation uncertainty.

<sup>#</sup> Stratigraphic units are labeled in Figures 6 and 23.

inundation. One gastropod was extracted 1-2 cm above the base of unit 3. A second gastropod was also collected 2-3 cm above the contact with unit 2 (Figure 6). This is probably because either (1) young gastropods burrowed down to the candidate tsunami sand, unit 2 or (2) the gastropods were contaminated with young carbon collected from an open system.

At Langi Bay, a wood fragment collected between subunits 2a and 2b in trench wall exposure A yielded a calibrated age range of 3690–3490 years B.P. (Figure 23 and Table 3). This older age may be a result of the 1861 tsunami scouring existing, older plants and trees and depositing them along with the sand at Langi Bay. Ambiguous radiocarbon ages can result from older, reworked carbon (Dawson, 1994; Goff *et al.*, 1998).

#### *Uranium–Thorium Dating*

Coral colonies such as the *Porites* or *Goniastrea* species have been analyzed using U–Th methods to determine the death of coral growth from coseismic emergence (Zachariasen *et al.*, 1999; Zachariasen *et al.*, 2000; Natawidjaja *et al.*, 2004; Meltzner *et al.*, 2006). Detrital coral blocks found on candidate tsunami sands can also be dated to determine the date of coral death.

Uranium–thorium geochronology uses the concentration ratios of uranium and thorium in the coral using inductively coupled plasma mass spectrometry (Shen *et al.*, 2002; Ku, 2000; Edwards *et al.*, 2003; Edwards *et al.*, 1988). The uranium–thorium method is based on the accumulation of decay products of U,  $^{230}\text{Th}$  and  $^{234}\text{U}$ , and gives the time at which uranium was incorporated into calcite. Uranium is dissolved in

seawater as the uranyl ion ( $\text{UO}_2^{2+}$ ) in oxidizing environments and attaches itself to carbonates by replacing the  $\text{Ca}^{2+}$  ion. Calculating the age of uranium incorporation takes into account the following assumptions: (1) at time zero, the  $^{230}\text{Th}$  concentration is zero and (2) the isotopic system is closed (Ku, 2000). A closed system implies no contamination, such as the incorporation of  $^{230}\text{Th}$  into the coral head during crystallization (Shen *et al.*, 2005).

The U–Th method is far more precise than radiocarbon dating because, for young corals (up to 1,000 years) an error as small as one year can be achieved (Shen *et al.*, 2005; Zachariasen *et al.*, 1999). At Busong Bay, in trench A, a 30 by 30cm coral block was collected from unit 3, above a very fine-grained bioturbated sand containing root fragments, unit 1 (Figure 26). X–Ray analysis of the coral block imaged coral growth rings (Figure 26), constraining the age of the coral head with respect to the U–Th determination. Eight spots were marked on the coral head, A1-A4 and B1-B4 (Figure 26). Specific regions on the coral head were chosen for U–Th analysis based on the amount of weathering. Weathering increases the amount of contamination by infiltration of foreign particles into the coral head (Shen *et al.*, 2005). For example, a sugary or powdery texture on the coral head indicates recrystallization that would compromise the U–Th analyses (Zachariasen *et al.*, 1999). Based on the lack of visible weathering, samples B1-B4 were chosen. Sample B3 yielded an uncorrected U–Th date of 1838 (Table 4).

I used a two-step approach to correct the U–Th analyses in the detrital coral sample. Since the error of the U–Th dating is typically within a few years for corals from

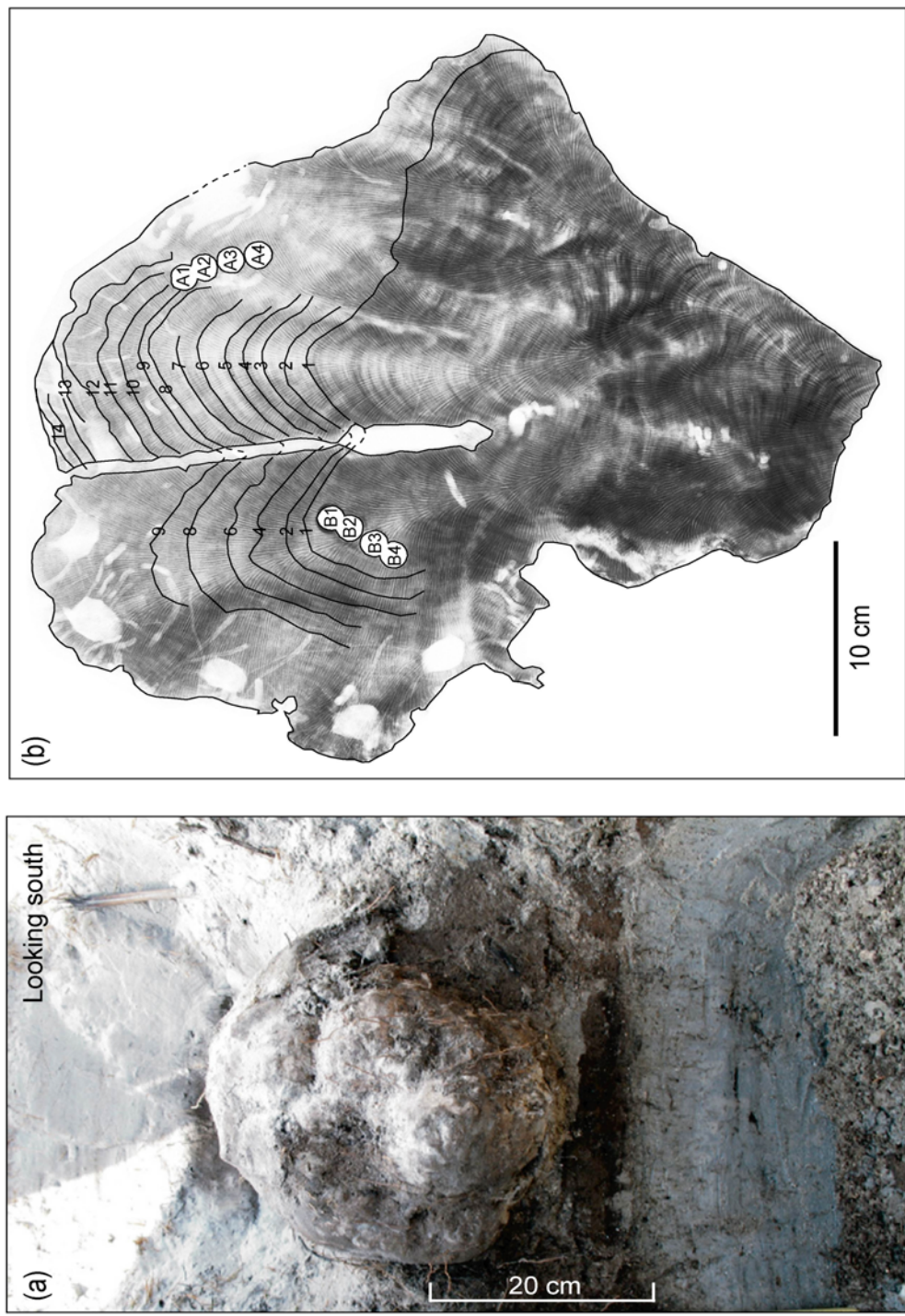


Figure 26. Busong Bay trench A U-Th sample. (a) Coral block that was collected for U-Th analysis, 55 m from the coastline (see Figure 18 for location) and (b) X-Ray image of coral block showing U-Th dating sample locations and numbered growth rings.

Table 4  
Uranium and Thorium Isotopic Compositions and  $^{230}\text{Th}$  Analyses

| Sample | $^{238}\text{U}$<br>ppb * | $^{232}\text{Th}$<br>ppt * | $\delta^{234}\text{U}$<br>measured <sup>†</sup> | $^{230}\text{Th}/^{238}\text{U}$ |                           | $^{230}\text{Th}$ Age<br>Uncorrected | $\delta^{234}\text{U}_{\text{initial}}$<br>corrected <sup>‡, §</sup> | Calendar<br>Year <sup>#</sup> |
|--------|---------------------------|----------------------------|---|----------------------------------|---------------------------|--------------------------------------|--|-------------------------------|
|        |                           |                            |   | Activity<br>Ratio <sup>‡</sup>   | Corrected <sup>‡, §</sup> |                                      |  |                               |
| GSG-3- | 2500 ± 3                  | 1689 ± 3                   | 144.2 ± 1.8                                     | 0.00177 ± 0.00004                | 169.2 ± 3.8               | 153.0 ± 18.5                         | 144.3 ± 1.8  | 1854 ± 19                     |
| B3     |                           |                            |   |                                  |                           |                                      |  | 1868 ± 19                     |

\* Under “ $^{232}\text{Th}$  ppb” and “ $^{232}\text{Th}$  ppt,” the ppb refers to parts per billion and the ppt refers to parts per trillion by mass.

$$\dagger \delta^{234}\text{U} = ([^{234}\text{U}/^{238}\text{U}]_{\text{activity}} - 1) \times 1000.$$

$$\ddagger [^{230}\text{Th}/^{238}\text{U}]_{\text{activity}} = 1 - e^{-\lambda 230T} + (\delta^{234}\text{U}_{\text{measured}}/1000)[\lambda_{230}/(\lambda_{230} - \lambda_{234})](1 - e^{-(\lambda_{230} - \lambda_{234})T}), \text{ where } T \text{ is the age.}$$

Decay constants are  $9.1577 \times 10^{-6}$  yr<sup>-1</sup> for  $^{230}\text{Th}$ ,  $2.8263 \times 10^{-6}$  yr<sup>-1</sup> for  $^{234}\text{U}$ , and  $1.55125 \times 10^{-10}$  yr<sup>-1</sup> for  $^{238}\text{U}$  (Cheng *et al.*, 2000).

§ Isochron Age; ages were calculated with the chemistry dates.

¶  $\delta^{234}\text{U}_{\text{initial}}$  corrected was calculated based on  $^{230}\text{Th}$  age (T), i.e.,  $\delta^{234}\text{U}_{\text{initial}} = \delta^{234}\text{U}_{\text{measured}} X e^{\lambda^{234} * T}$ , and T is corrected age.

# The 1854 is determined by subtracting the corrected  $^{230}\text{Th}$  age from the time of analysis (2007); the year 1868 in italics is determined by counting annual bands visible in X-Ray. This method was adapted from Natawidjaja *et al.*, 2004.

0 to 1,000 years old (Edwards *et al.*, 1988; Zachariasen *et al.*, 1999), we subtract the  $^{230}\text{Th}$  age from the time of analysis (i.e., 2007). This yields an age of  $1854 \pm 19$  years.

Second, we added the 14 annual coral growth bands visible in X-Ray analysis (Figure 26) to the corrected U–Th age. This yields an age of  $1868 \pm 19$  (at  $2\sigma$ ) for the timing of the coral head death (Table 4). The error of 19 years is the 2 sigma uncertainty calculated by the following equation:

$$\sqrt{(a^2 + b^2)} \quad (3)$$

where  $a$  is 18.5 years, the U–Th analytical error, and  $b$  is 6 years, the error associated with counting annual growth rings (Figure 26). The U–Th dating was completed at the University of Minnesota, Minneapolis Isotope Laboratory, Department of Geology and Geophysics.

#### Topographic Profiling

Topographic profiles were completed to characterize the local geomorphic setting of each field site. Tsunami sand elevations and topographic profiles were measured using a Total Station and a hydrographic tube. To provide a local height datum, relative elevations of paleo-beach ridges and modern shorelines from Total Station and GPS data were tied into global mean sea level by the program “NLOADF” (Agnew, 1997). Topographic profiles starting at the water’s edge were taken that tied the relative sea level with geomorphic features and stratigraphic layers documented in trench wall exposures. At each field site, the date, the time of day, and the specific latitude and longitude of the tidal measurement locations were recorded. NLOADF gives the tidal elevations for each field site at the specific date and time the elevation measurements were obtained,

allowing for a local height datum. The difference in elevation from the measured tide and the actual tide were then incorporated into the geomorphic maps. Once a height datum is obtained, the relative depth of specific layers within excavations to the tides, such as candidate tsunami sands, can be established. Although not as accurate as emergence determined by coral microatoll studies (Zachariasen *et al.*, 1999), tsunami sand elevation can determine if the region has undergone emergence or subsidence.

Topographic profiles perpendicular to the beach at Inor (Figure 4), Busong Bay (Figure 18), and Langi Bay (Figure 21) tied the elevation of the 2004 and 1861 tsunami sands to the 2006 annual low tide at Inor (Figure 27), Busong Bay (Figure 28), and Langi Bay (Figure 27) (Table 5). At Inor, the 1861 tsunami sand deposit is between 3.4 and 4.2 m above the 2006 annual low tide (Figure 27). The 2004 tsunami horizon is between 3.5 and 4.5 m above the 2006 annual low tide at Inor (Figure 27). At Busong Bay, the 2004 tsunami sand is between 2.1 and 3.3 m above the 2006 annual low tide (Figure 28). The 1861 tsunami sand is between 1.5 and 1.8 m above the 2006 annual low tide at Busong Bay (Figure 28). At Langi Bay, the 2004 tsunami sand was 0.8 m above the 2006 annual low tide (Figure 27). The candidate 1861 tsunami sand layer was 1.5 m above the 2006 annual low tide at Langi Bay (Figure 27).

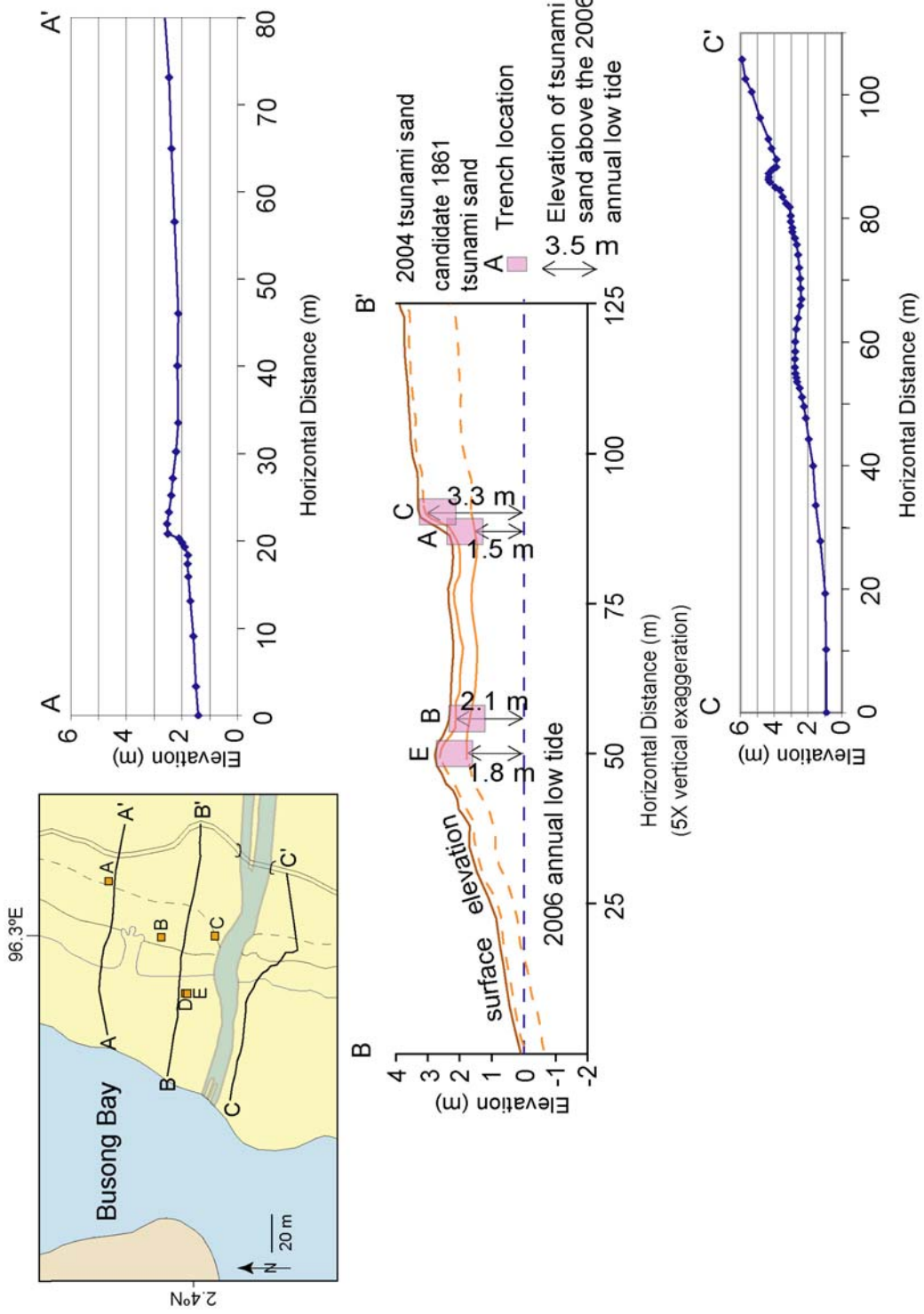


Figure 27. Langi Bay and Inor topographic profiles. (a) Langi Bay location map and profiles A–A' and B–B'. (b) Inor location map and profile A–A'; tsunami horizons in relation to the 2006 annual low tide.

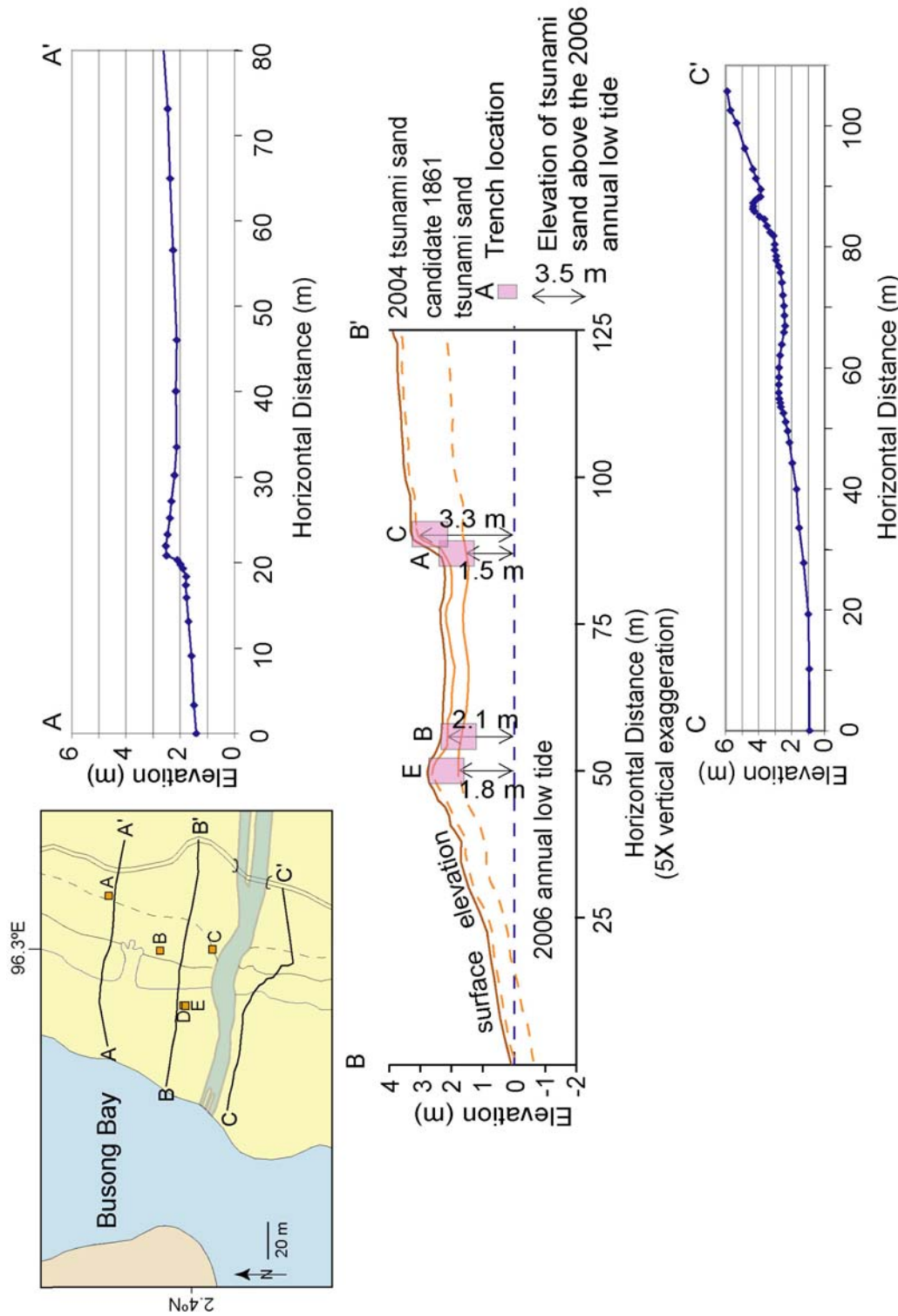


Figure 28. Busong Bay topographic profiles; tsunami depths in relation to the 2006 annual low tide.

Table 5  
Heights of the Candidate 1861 and 2004 Tsunami Sands Above  
the 2006 Annual Low Tide

| Trench wall<br>excavation      | Inor |     |     |     |     | Langi Bay |     |     | Busong Bay |     |     |     |
|--------------------------------|------|-----|-----|-----|-----|-----------|-----|-----|------------|-----|-----|-----|
|                                | A    | B   | D   | E   | F   | A         | D   | E   | A          | B   | C   | E   |
| Candidate 1861<br>tsunami sand | 3.4  | 3.5 | 4.0 | 4.2 | 3.8 | 1.5       | –   | 1.5 | 1.5        | 1.6 | 1.6 | 1.8 |
| 2004 tsunami sand              | 3.7  | 4.7 | 4.4 | 4.5 | 4.1 | 1.7       | 0.8 | 2.2 | 2.2        | 2.1 | 3.3 | 2.6 |

## CHAPTER III

### DISCUSSION

Three field sites, Busong Bay, Langi Bay, and Inor show evidence of the 2005 and 2004 and past tsunamis. Tsunami sands found in trench wall exposures on Simeulue Island represent tsunamis generated in the aftermath of the December 26, 2004  $M_w$  9.2 and February 16, 1861  $M_w$  ~8.5 earthquakes. The 2004 and 1861 tsunamis resulted in the deposition of large coral boulders at Busong Bay (Figure 20).

#### The 2004 Tsunami Deposits

The 2004 tsunami sand deposits within trench wall exposures range in thickness from a few millimeters to 30 cm and are relatively inconsistent throughout the three field sites. At Busong Bay, the 2004 tsunami sand layer is the thickest and best represented of the three field sites. The tsunami sand thickness varies within the trench wall exposures, between 20 and 30 cm (Figures 19 and 29). The 2004 sand consists of 6 subunits (subunits 5a-f; Figures 19 and 29) that most likely represent consecutive waves of the tsunami event (Dawson *et al.*, 1994; Goff *et al.*, 1998; Moore *et al.*, 2006). For example, on mainland Sumatra, near Banda Aceh, the 2004 tsunami deposit was up to 80 cm thick.

In Banda Aceh, the laminated sand was deposited by three consecutive waves (Moore *et al.*, 2006). Most of the tsunami deposits were normally graded, although massive and inverse grading was also observed (Moore *et al.*, 2006). The tsunami deposits may have been thicker at Banda Aceh due to a larger nearby sediment source compared to Busong Bay, Simeulue Island.

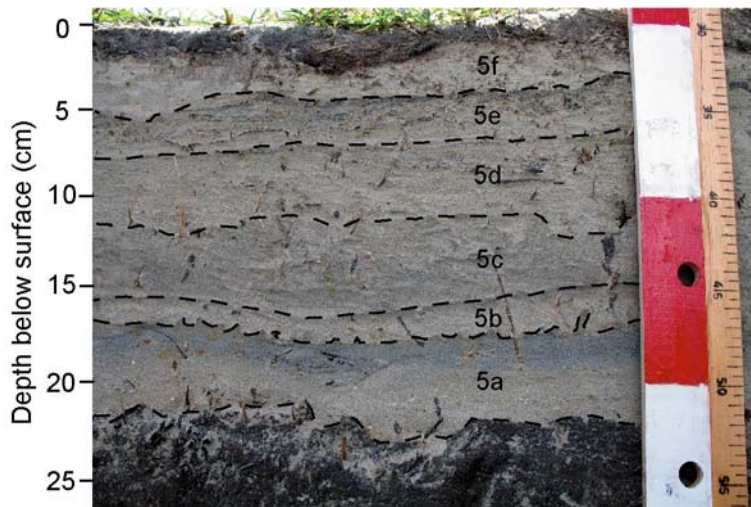


Figure 29. Busong Bay trench B showing sub-layers and minor flame structures within the 2004 tsunami sand, looking north (see Figure 18 for trench location).

At Langi Bay, unit 3 in trench wall exposure D, the sand deposited by the 2004 tsunami is from 9 to 15 cm thick in trench wall exposures. Unit 3 consists of fining upward fine to very fine sand that contains plastic rip-up clasts (Figure 24). Previous studies in Sumatra from the 2004 tsunami (Moore *et al.*, 2006), tsunami deposits in New Zealand of various ages (Goff *et al.*, 2001), and the 1998 tsunami deposits in Papua New Guinea (Gelfenbaum and Jaffe, 2003) show evidence of tsunami sands fining upwards. As the velocity of the tsunami decreases, particle grain size also decreases, recorded in normally graded beds. Similar sequences exist from turbidite deposits (Boggs, 2001). Rip-up clasts indicate the erosive and destructive nature of the tsunami (Gelfenbaum and Jaffe, 2003). At Inor, the 2004 tsunami sand is massive, well sorted, and 0 to 5 cm thick (Figures 6, 7, and 8).

Variations in the 2004 tsunami sand thickness from site to site may be the result of obstructions, such as trees or buildings and local topography. For example, at Inor, the 2004 tsunami had to move through houses and trees before depositing sand in the rice

paddies. In contrast, Busong Bay and Langi Bay do not have such obstructions between the shoreline and the study area.

Based on the wave height and wavelength, the velocity of the tsunami near Banda Aceh may have reached 10 m/s, with inland inundation up to 5km (Moore *et al.*, 2006). The 2004 tsunami deposit at Busong Bay is marked by large coral boulders, up to 5m in diameter, deposited up to 75m inland from the modern shoreline (Figures 4 and 23). It is common for strong tsunamis to deposit large boulders inland. Coral boulders 1m in diameter were deposited up to 200m inland from the tsunami generated by rupture of the Sunda megathrust during the December 12, 1992  $M_w$  7.5 earthquake in Flores, Indonesia (Shi and Smith, 2003). The tsunami run-up heights during the Flores earthquake were 26m (Shi and Smith, 2003).

#### The Candidate 1861 Tsunami Deposits

At Busong Bay, the candidate 1861 tsunami deposit is documented in numerous trench wall exposures. The candidate 1861 tsunami sand deposit at Busong Bay is between 9 and 47 cm thick (Figure 19) and is located at least 125 m inland based on the inland extent of coral boulders up to 7m in diameter deposited on the land surface (Figures 18 and 20). The U–Th date of death of a coral boulder found directly on top of a candidate tsunami sand in trench A at Busong Bay was  $1868 \pm 19$  years (Figure 26 and Table 4). This date of coral death brackets the 1861 earthquake and tsunami.

The *Porites* or *Goniastrea* species of corals cannot live above annual lowest tides, known as highest level of survival (HLS), because exposure to sunlight for extended amounts of time proves fatal (Zachariasen *et al.*, 1999). Therefore, constraining the time

of coral death records the exposure to sunlight from rapid coseismic emergence, tsunami inundation, or both. A tsunami can cause the death of a coral head by detaching it and depositing the coral head inland.

At Langi Bay, the candidate 1861 tsunami sand layer is between 20 and 26cm thick, with 2 subunits that fine upwards (Figure 23). Although the modern radiocarbon date from trench A does not offer additional age constraints, the tsunami deposits at Langi Bay are very similar to those at Inor. For example, both sites show fining upward subunits that are weakly laminated within the tsunami sand (Figures 6 and 23). In addition, the units from Inor and Langi Bay bracketing the 1861 tsunami are likely correlative.

At Inor, the candidate 1861 tsunami sand is between 5 and 15cm thick within trench wall exposures 360m inland from the modern shoreline (Figures 4 and 5-10). Rip-up clasts, a common feature representing the erosive nature of tsunamis, are present in unit 2 within trench wall exposures at Inor (Figures 30 and 31). The grain size distribution and bioclastic material from unit 2 trench wall exposures and the nearby beach sand at Inor are difficult to differentiate and were likely derived from a shallow marine depositional environment (Figures 14-16). Northward from the modern shoreline at Inor, the tsunami sand grain size decreases from 2.1  $\Phi$  to 3.3  $\Phi$ , mud weight percent increases, and bioclastic material decreases (Figures 4 and 14-16). These changes indicate a weakening of the tsunami wave(s) upon moving inland. The variations in mud weight percent may represent both run-up and backwash resulting from the tsunami wave train.

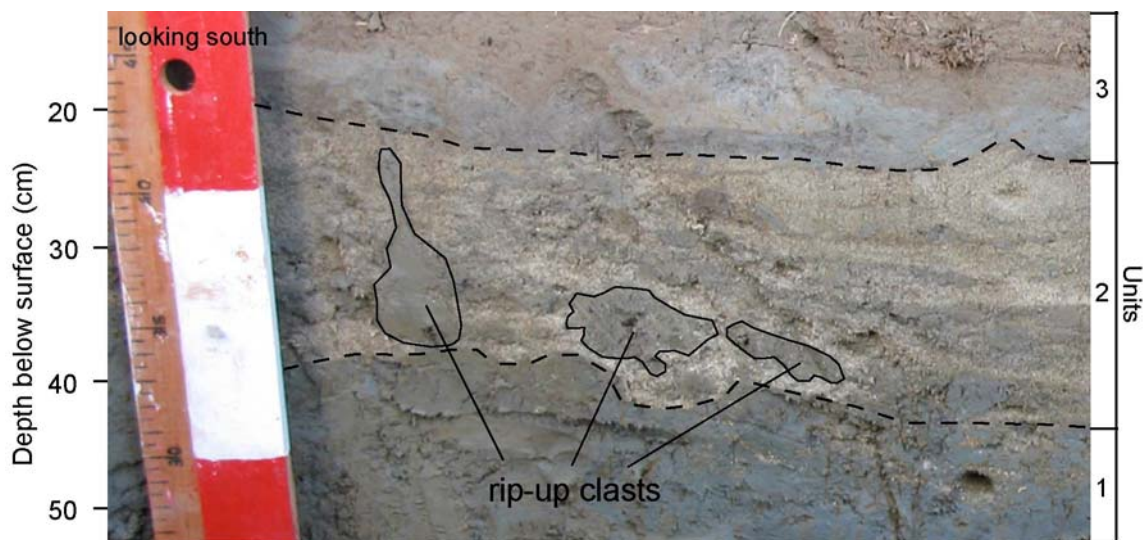


Figure 30. Rip-up clasts at the base of unit 2, trench E, Inor. The rip-up clasts were derived from unit 1 (see Figure 4 for trench location).

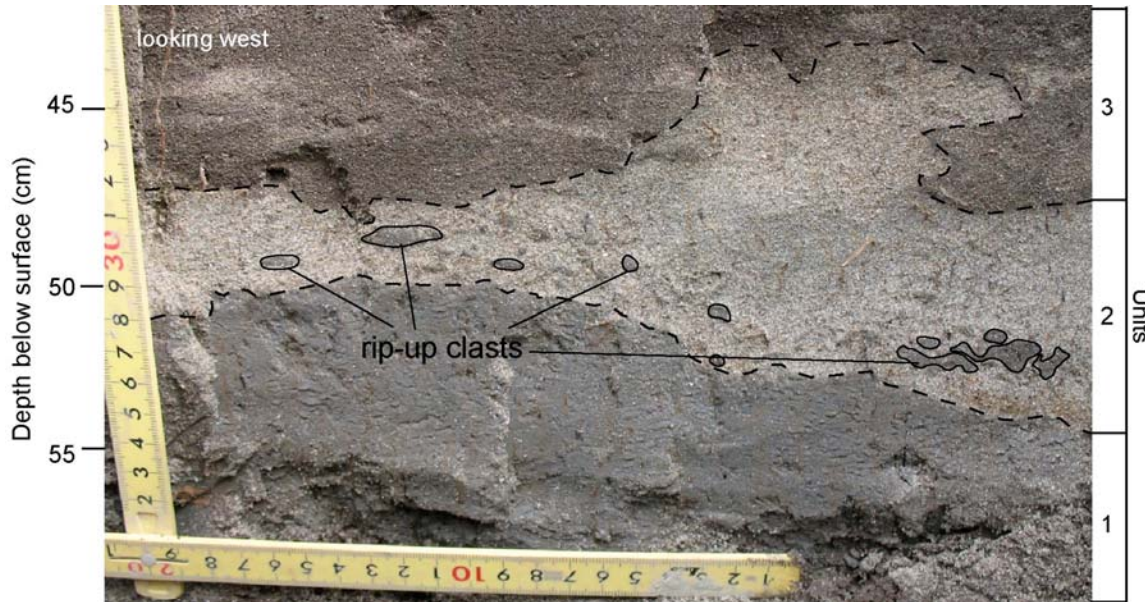


Figure 31. Rip-up clasts within unit 2, trench F, Inor. The rip-up clasts were derived from unit 1 (see Figure 4 for trench location).

For example, analyses of tsunami deposits from the Second Storegga submarine landslide 7,000 B.P. (Dawson *et al.*, 1988) by Shi *et al.* (1991) include a series of fining upwards sequences that are thought to be from individual waves.

#### Tsunami Sands and Coseismic Uplift

Rupture during the 2004 earthquake produced a maximum vertical displacement of about 11m (Briggs *et al.*, 2006), resulting in the displacement of ocean water producing the tsunami.

Tsunamis have been observed along subduction zones worldwide. For example, following the  $M_w$  9.5 Chile earthquake, up to 4 tsunami waves were observed, inundating up to 2km inland (Wright and Mella, 1963). In addition, this tsunami had wave heights up to 15m above mean sea level in the open ocean (Wright and Mella, 1963). In Japan, there are accounts of tsunamis from numerous earthquakes, including the  $M_w$  8.5 1854 earthquake that produced wave heights up to 7m along the eastern coastline of Japan (Takashimizu and Masuda, 2000). The 1700 Cascadia  $M_w$  9.0 earthquake produced tsunamis throughout the Pacific Ocean, including Japan (Atwater *et al.*, 2005). Most recently, tsunamis throughout the Indian Ocean were observed from the 2004  $M_w$  9.2 Sumatran earthquake (Moore *et al.*, 2006).

Although the  $M_w$  ~8.5 1861 earthquake was substantially smaller than the 2004  $M_w$  9.2 earthquake, tsunami sand thickness and coral boulder deposition indicate that the 1861 tsunami run-up heights were greater than the 2004 run-up heights. In 2004, local residents stated that tsunami heights reached 2m. Based on eyewitness reports, in 1861, tsunami heights were up to 7m in some areas (Newcomb and McCann, 1987).

The rupture patch from the 1861 earthquake closely resembles that of the  $M_w$  8.7 March 28, 2005 rupture patch (Figure 2). Therefore, the amount of uplift from the 2005 earthquake will be assumed for the 1861 earthquake. Furthermore, since the 2005 tsunami sand is only located at Busong Bay (Figure 19) and both the 2004 and 1861 tsunami sands are represented at all three field sites, the 2004 and 1861 tsunami sands were compared.

In 2005, northwest Simeulue Island (Langi Bay) had zero uplift while southeast Simeulue Island (Busong Bay) experienced about 1.5m of uplift (Figure 2). The 1861 tsunami sand deposit is between 9 and 15cm thick at Busong Bay (Figure 19) and between 20 and 26cm thick at Langi Bay (Figure 23). The thicker deposit at Langi Bay may be the result of less coseismic uplift. During the 2004 earthquake, Langi Bay underwent coseismic uplift (Figure 2) and has a tsunami sand deposit from 11 to 15cm thick (Figure 23). At Busong Bay, the 2004 tsunami sand is between 20 and 30cm thick (Figure 19) and experienced coseismic subsidence (Figure 2). My field sites show a clear correlation between coseismic land level changes and tsunami sand thickness (Figure 32). Coseismic uplift results in the deposition of a thinner sand layer while subsidence produces a thicker sand deposit.

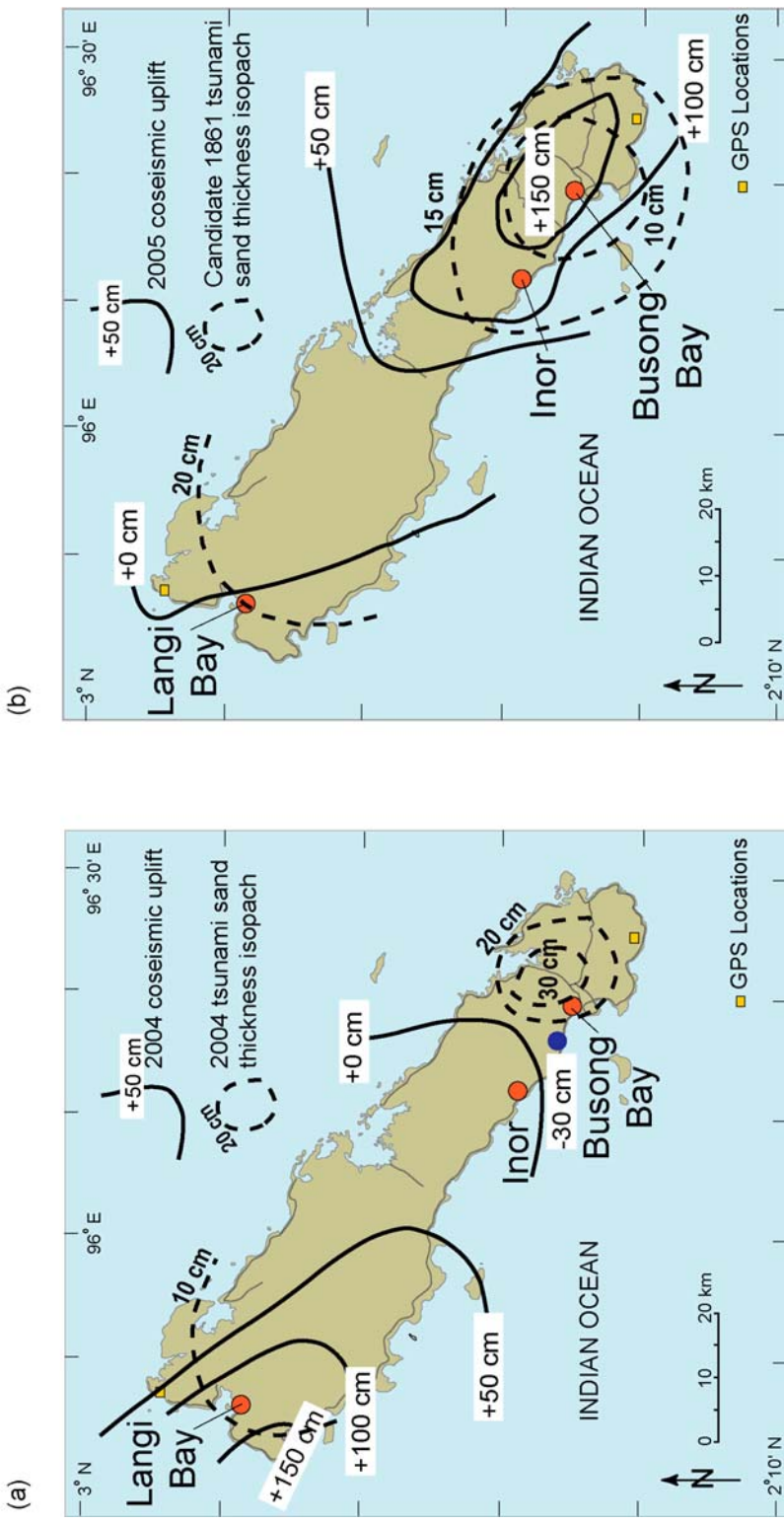


Figure 32. Coseismic land level changes and tsunami sand thickness isopachs on Simeulue Island. (a) Uplift and subsidence associated with the 2004 earthquake and the 2004 tsunami sand thickness. (b) Uplift associated with the 2005 earthquake and the candidate 1861 tsunami sand thickness; land level changes from the 2005 earthquake are assumed for the 1861 earthquake to compare the candidate 1861 tsunami sand deposits with the 2004 deposits; the 2005 tsunami sand was not found throughout Simeulue Island.

## CHAPTER IV

### CONCLUSIONS

AMS analyses of wood fragments from Inor and Langi Bay and U/Th analysis of a coral boulder from Busong Bay yielded ages that bracket the 1861 tsunami. Trench wall stratigraphy at Inor, Busong Bay, and Langi Bay show that in 1861, tsunami inundation was at least 350m inland and deposited up to 26cm of sand. Excavations and coral boulders at Busong Bay show that the 2004 tsunami inundated Simeulue Island at least 60m inland and deposited up to 30cm of sand. Variations in local topography and structures may affect the thickness of tsunami deposits from site to site. Sedimentary structures in both the 1861 and 2004 tsunami sands, such as rip-up clasts and flame structures, show the erosive nature of tsunami waves. Subunits within tsunami sands may indicate consecutive waves in the tsunami wave train.

## REFERENCES

- Agnew, D. C. (1997). NLOADF: a program for computing ocean-tide loading, *J. Geophys. Res.* **102**, 5109-5110.
- Atwater, B. F. and A. L. Moore (1992). A tsunami about 1000 years ago in Puget Sound, Washington, *Science* **258**, 1614-1617.
- Atwater, B. F., S. Musumi-Rokkaku, S. Kenji, T. Yoshinobu, U. Kazue, and D. K. Yamaguchi (2005). The Orphan Tsunami of 1700, Japanese clues to a parent earthquake in North America, *U. S. Geol. Surv. Prof. Paper 1707*, 133 pp.
- Benson, B. E., K. A. Grimm, and J. J. Clague (1997). Tsunami deposits beneath tidal marshes on northwestern Vancouver Island, British Columbia, *Quat. Res.* **48**, 92-204.
- Bilham, R. (2007). Personal Communication.
- Bilham, R., E. R. Engdahl, N. Feldl, and S. P. Satyabaka (2005). Partial and complete rupture of the Indo-Andaman plate boundary 1847-2004, *Seism. Res. Lett.* **76**, 299.
- Bock, Y., L. Prawirodirdjo, J. F. Genrich, C. W. Stevens, R. McCaffrey, C. Subarya, S. S. O. Puntodewo, and E. Calais (2003). Crustal motion in Indonesia from Global Positioning System measurements, *J. Geophys. Res.* **108(B8)**, B000324.
- Boggs, S., Jr. (2001). *Principles of Sedimentology and Stratigraphy, Third Edition*, Prentice Hall, 59-87.
- Briggs, R. W., K. Sieh, A.J. Meltzner, D. H. Natawidjaja, J. Galetzka, B. Suwargadi, Y. Hsu, M. Simons, N. Hananto, I. Suprihanto, D. Prayudi, J.-P. Avouac, L. Prawirodirdjo, and Y. Bock (2006). Deformation and slip along the Sunda megathrust in the great 2005 Nias-Simeulue earthquake, *Science* **311**, 1897-1901.
- Bronk Ramsey, C. (2005). *Oxcal Program V. 3.10*, University of Oxford Radiocarbon Unit, Oxford.
- Bryant, E. (1997). *Climate Process and Change*, Cambridge University Press, Cambridge, 40-42.
- Cheng, H., R. L. Edwards, J. Hoff, C. D. Gallup, D. A. Richards, and Y. Asmerom (2000). The half-life of uranium-234 and thorium-230, *Chem. Geol.* **169**, 17-33.

- Cisternas, M., B. F. Atwater, F. Torrejon, Y. Sawai, G. Machuca, M. Lagos, A. Eipert, C. Youlton, I. Salgado, T. Kamataki, M. Shishikura, C. P. Rajendran, J. K. Malik, Y. Rizal, and M. Husni (2005). Predecessors of the giant 1960 Chile earthquake, *Nature* **437**, 404-407.
- Dawson, A. (1994). Geomorphologic effects of tsunami run-up and backwash, *Geomorph.* **10**, 83-94.
- Dawson, A. G., I. D. L. Foster, S. Shi, D. E. Smith, and D. Long (1988). The Storegga Slides: evidence from eastern Scotland for a possible tsunami, *Mar. Geol.* **82**, 271-276.
- DeShon, H. R., E. R. Engdahl, C. H. Thurber, and M. Brudzinski (2005). Constraining the boundary between the Sunda and Andaman subduction systems: Evidence from the 2002 Mw Northern Sumatra earthquake and aftershock relocations of the 2004 and 2005 great earthquakes, *Geophys. Res. Lett.* **32**, L24307.
- Dewey, J. W., G. Choy, B. Presgrave, S. Sipkin, A. C. Tarr, H. Benz, P. Earle, and D. Wald (2007). Seismicity associated with the Sumatra-Andaman Islands earthquake of 26 December 2004, *Bull. Seism. Soc. Am.* **97**, S25-S42.
- Edwards, R. L., C. D. Gallup, and H. Cheng (2003). Uranium-series dating of marine and lacustrine carbonates, *Rev. in Mineral. and Geochem.* **52**, 363-405.
- Edwards, R. L., F. W. Taylor, and G. J. Wasserburg (1988). Dating earthquakes with high-precision thorium-230 ages of very young corals, *Earth and Plan. Science Lett.* **90**, 371-381.
- Gelfenbaum, G. and B. Jaffe (2003). Erosion and Sedimentation from the 17 July, 1998 Papua New Guinea tsunami, *Pure Appl. Geophy.* **160**, 1969-1999.
- Goff, J., C. Chagué-Goff, and S. Nichol (2001). Paleotsunami deposits: a New Zealand perspective, *Sediment. Geol.*, **143**, 1-6.
- Goff, J. R., M. Crozier, V. Sutherland, U. Cochran, and P. Shane (1998). Possible tsunami deposits of the 1855 earthquake, North island, New Zealand. *Coast. Tect.*, Stewart I. S., Vita-Finzi, C. (Eds.), *Geol. Soc. Spec. Publ.* No. 133, 353-374.
- Jhingram, A.G. (1953). A note on the earthquake in the Andaman Islands (26 June 1941). *Rec. Geol. Surv. India*, **82**, 300-307.
- Kelsey, H. M., A. R. Nelson, E. Hemphill-Haley, and R. C. Witter (2005). Tsunami history of an Oregon coastal lake reveals a 4600 yr record of great earthquakes on the Cascadia subduction zone, *Geol. Soc. Am. Bull.* **117**, 1009-1032.

- Krishnan, R. (1953). General Report for 1941. *Rec. Geol. Surv. India*, **79**, 193-194.
- Krumbein, W.C. (1934). Size frequency distribution of sediments, *J. Sedim. Petr.* **4**, 65-77.
- Ku, Te-Lung (2000). Uranium-Series Methods: in Quaternary Geochronology: Methods and Applications, (editors: Noller, J.S., Sowers, J.M., and Lettis, W.R.), *Am. Geophys. Un.* 101-114.
- McCloskey, J., S. Nalbant, and S. Steacy (2005). Indonesian earthquake: Earthquake risk from co-seismic stress, *Nature* **434**, 291.
- Meltzner, A. J., K. Sieh, M. Abrams, D. C. Agnew, K. W. Hudnut, J.-P. Avouac, and D. H. Natawidjaja (2006). Uplift and subsidence associated with the great Aceh-Andaman earthquake of 2004, *J. Geophys. Res.* **111**, B02407.
- Minoura, K., V. G. Gusiakov, A. Kurbatov, S. Takeuti, J. I. Svendsen, S. Bondevik, and T. Oda (1996). Tsunami sedimentation associated with the 1923 Kamchatka earthquake, *Sedim. Geol.* **106**, 145-154.
- Minoura, K., H. Yamauchi, K. Fujioka, and M. Shiba (1988). Newly-designed grain-size analyzer with settling tube system and its application to bottom sediments of Mutsu Bay, *Sci. Rp., Hirosaki Univ.* **35**, 50-63 (in Japanese with English abstract).
- Moore, A., Y. Nishimura, G. Gelfenbaum, T. Kamataki, and R. Triyono (2006). Sedimentary deposits of the 26 December 2004 tsunami on the northwest coast of Aceh, Indonesia, *Earth Planets Space* **58**, 253-258.
- Morton, R. A., G. Gelfenbaum, and B. E. Jaffe (2007). Physical criteria for distinguishing sandy tsunami and storm deposits using modern examples, *Sed. Geol.*, *in press*.
- Nanayama, F., K. Satake, R. Furukawa, K. Shimokawa, B. F. Atwater, K. Shigeno, and S. Yamaki (2003). Unusually large earthquakes inferred from tsunami deposits along the Kuril trench, *Nature* **424**, 660-663.
- Natawidjaja, D. H., K. Sieh, S. N. Ward, H. Cheng, R. L. Edwards, J. Galetzka, and B. W. Suwargadi (2004). Paleogeodetic records of seismic and aseismic subduction from central Sumatran microatolls, Indonesia: *J. Geophys. Res.* **109**, B04306.
- Newcomb, K. R. and W. R. McCann (1987). Seismic history and seismotectonics of the Sunda Arc, *J. Geophys. Res.* **92**, 421-440.

- Reading, H. G. (1996). *Sedimentary Environments: Processes, Facies and Stratigraphy, Third Edition*, Blackwell Science Ltd., 37-82 and 154-231.
- Rivera, L., K. Sieh, D. Helmberger, and D. H. Natawidjaja (2002). A comparative study of the Sumatran subduction-zone earthquakes of 1935 and 1984, *Seismol. Soc. Am. Bull.* **92**, 1721-1736.
- Shen, C., R. L. Edwards, H. Cheng, J. A. Dorale, R. B. Thomas, S. B. Moran, S. E. Weinstein, and H. N. Edmonds (2002). Uranium and thorium isotopic and concentration measurements by magnetic sector inductively coupled plasma mass spectrometry, *Chem. Geol.* **185**, 165-178.
- Shen, C., K. Li, K. Sieh, D. Natawidjaja, X. Wang, H. Cheng, and R. L. Edwards (2005). Limits and applications of high precision coral Th-230 dating techniques (abstract), PP21C-1573.
- Shi, S. A. G. Dawson, D. E. Smith (1991). Sedimentology of a Holocene tsunami deposit, *Abstr. XIII Int. Congr. of the International Union for Quat. Res. (INQUA)*, Beijing, China, August 2-9, 1991, 329.
- Shi, S. and D. E. Smith (2003). Coastal tsunami geomorphological impacts and sedimentation processes: Case studies of modern and prehistorical events, International Conference on Estuaries and Coasts, Hangzhou, China.
- Stuiver, M. and H. A. Polach (1977). Discussion: reporting of  $^{14}\text{C}$  data, *Radiocarbon* **19**, no. 3, 355-363.
- Subarya, C., M. Chlieh, L. Prawirodirdjo, J.-P. Avouac, Y. Bock, K. Sieh, A. J. Meltzner, D. H. Natawidjaja, and R. McCaffrey (2006). Plate-boundary deformation associated with the great Sumatran-Andaman earthquake, *Nature* **440**, 46-51.
- Takashimizu, R. and F. Masuda (2000). Depositional facies and sedimentary successions of earthquake-induced tsunami deposits in upper Pleistocene incised valley fills, central Japan, *Sediment. Geol.* **104**, 175-188.
- Walker, K. T., M. Ishii, and P. M. Shearer (2005). Rupture details of the 28 March 2005 Sumatra Mw 8.6 earthquake imaged with teleseismic P waves, *Geophys. Res. Lett.* **32**, L24303.
- Woodroffe, C. D. (2003). *Coasts: Form, Process and Evolution*, Cambridge University Press, Cambridge, 378-434.

- Wright, C. and A. Mella (1963). Modifications to the soil pattern of South-central Chile resulting from seismic and associated phenomena during the period May to August 1960, *Seism. Soc. Am. Bull.*, **53**, 1367-1402.
- Yulianto, E. (2006). Personal Communication.
- Zachariasen, J., K. Sieh, F. W. Taylor, R. L. Edwards, and W. S. Hantoro (1999). Submergence and uplift associated with the giant 1833 Sumatran subduction earthquake: Evidence from coral microatolls, *J. Geophys. Res.* **104**, 895-919.
- Zachariasen, J., K. Sieh, F. Taylor, and W. S. Hantoro (2000). Modern vertical deformation at the Sumatran subduction zone, Paleogeodetic Insights from Coral Microatolls, *Seism. Soc. Am. Bull.* **90**, 897-913.